Author's response to the final comments on the manuscript:

Estimation of the total magnetization direction of approximately spherical bodies

V. C. Oliveira Jr.[1], D. P. Sales[1], V. C. F. Barbosa[1], and L. Uieda[1, 2]

[1]Observatório Nacional, Brazil

[2]Universidade do Estado do Rio de Janeiro, Brazil

We would like to thank the Editor and the referees for their constructive review.

The last version of the manuscript has been revised. We have incorporated most of corrections recommended by reviewers. Below we comment in detail on the recommendations and questions raised by reviewers.

General comments to the authors:

I feel I must begin with a brief apology to the authors. I was under the impression that this would be a more open back-and-forth discussion of your work, with more chance for short responses to allow clarification. As such, my original review comments were brief and intended to spur collegial discussion rather than more heated discourse. My comments below will be more detailed to avoid any misunderstandings.

To summarize, I think this is a well thought through manuscript, with good synthetic work to validate the methods and assess their advantages and limitations. While the synthetic tests are well thought through and provide much information on the behaviour of the proposed method, I do not think they are sufficient. Unfortunately there are some similarities with other works that need to be addressed. My other major concern is with respect to application to real data examples. My comments below will speak to these major concerns.

However, I should first clarify some of my previous points as I do not think you have understood my meanings or intent entirely. My comments regarding the similarity of your methods to those of Lelievre & Oldenburg (2009) and Ellis et al. (2012) were with respect to the actual numerical problem being solved. Of course the intended practical application of

both approaches are wholly different are you have done a good job explaining this to me. You are solving a numerical problem that is essentially identical to what Lelievre & Oldenburg (2009) and Ellis et al. (2012) would end up with were they to remove many cells from their meshes, and thereby obtain a very small full sensitivity matrix with three rows for each remaining cell (equivalent to your separated dipole sources) and also remove all regularization from the problem. This comment is perhaps too academic and abstract to be completely fair. What I was trying to get at was that it seems out-of-place for you to be using similar numerical solution algorithms that are also used for much larger numerical problems of a similar numerical nature. You are dealing with much smaller problems so why not apply global optimization methods that can provide likelihood information? Please address this in your manuscript.

We will not continue debating the differences between our method and the methods proposed by Lelièvre & Oldenburg (2009) and Ellis et al. (2012). In the last review, we presented an in depth discussion about these differences.

We focus on your question: *"why not apply global optimization methods that can provide likelihood information?"*

Response: Yes, we can use a global optimization method as well as other methods too. We have chosen to follow the optimization methods shown in our manuscript because they work very well. Only in this manuscript we present the results of 202 inversions confirming the efficiency of the used optimization methods.

It is important that you mention the work below and other work in the field of UXO detection: L. R. Pasion. Inversion of time-domain electromagnetic data for the detection of unexploded ordnance. PhD thesis, University of British Columbia, 2007. In that work, Pasion inverts magnetic data for a best fitting dipole, the parameters being the location (x,y,z), the magnetization (mx,my,mz) and a dc offset for the data. This makes it a more complicated problem than what you are attempting to solve, and makes your problem a simplification of his. Therefore, what you need to do in your manuscript is compare your methods to his, or other work like his, and explicitly indicate what you are doing that is new or different. What I see as being different in your work is that you are supplying the location information as prior information to the inversion. I think it is critical that you compare against the already published work of Pasion.

We disagree with you. In our manuscript, we are inverting total-field anomaly. Rather, in the work in this thesis the author inverts TEM data and magnetic induction. Hence, a comparison of our work with the mentioned Phd Thesis is outside the scope our manuscript.

Although we do not add this reference, we have added a recent paper that presents an outstanding and comprehensive review of methods that determine the remanent and total magnetizations of magnetic sources. This paper is

Clark D. D. (2014) Methods for determining remanent and total magnetisations of magnetic sources – a review, Exploration Geophysics, 2014, 45, 271–304, doi: 10.1071/EG14013

I still must hold fast to my comments regarding the applicability of your methods. Yes, they are more computationally feasible than a fine mesh-based inversion for a discretization of magnetization. However, there are clearly assumptions that must be made about the subsurface in order to apply your methods. You say I am confusing assumed premise and prior information. No, they are closely related. Any assumed premise in your inversion methods means they can only be safely applied to problems in which that assumed premis holds. For example, a linear magnetic inversion that assumes low susceptibilities is not applicable to a magnetic problem in which one knows there are significant high susceptibilities and non-linear self-demagnetization effects. If you are going to apply any inversion methods to a particular problem then you must have sufficient a priori information to allow application of those methods. However, I do take your arguments into consideration and allow that it is sometimes acceptable to apply an inversion method where the assumed premise fails, but one must be asking appropriate exploration questions. For example, you mention that you can apply your methods to any shape of body provided you upward continue the data enough such that the response becomes more dipole-like. However, that approach can only provide a single magnetization direction within that body, so this is really only appropriate if the exploration question is to determine the average magnetization direction within a body. I think you should mention that in your conclusions.

We fully agree with you. Our approach assumes sources with constant magnetization direction. In our manuscript, this aspect is written in the methodology, tests and in the conclusion sections. In this new version of the manuscript, we also added this information in the abstract section and a new sentence in the conclusion section.

You must also have a reliable estimate of the number of sources and their locations (lateral and depth). There is little in your manuscript that attends to the former problem (how many sources exist). Other researchers have investigated problems in which they attempt to determine the number of dipole sources or fit several dipole bodies to overlapping data responses. Here are two relevant references:

S. D. Billings and F. Herrmann. Automatic detection of position and depth of potential UXO using continuous wavelet transforms. In Proceedings of SPIE, Detection and Remediation Technologies for Mines and Minelike Targets VII, 2003.

No action was taken. According to the *Manuscript preparation guidelines for authors* (http://www.nonlinear-processes-in-geophysics.net/for_authors/manuscript_preparation.html), *"Papers should make proper and sufficient reference to the relevant formal literature. Informal or so-called "grey" literature may only be referred to if there is no alternative from the formal literature"*. In our opinion, this reference is not part of "*the relevant formal literature*" and is not accessible to the reader.

Song, L., L. R. Pasion, S. D. Billings, and D. W. Oldenburg, 2011, Nonlinear inversion for multiple objects in transient electromagnetic induction sensing of unexploded ordnance: Techniques and applications: IEEE Trans. on Geoscience and Remote Sensing, 49, no. 10, 4007-4020.

Actually, we need to yield the number of sources and their locations. The number of sources is a subjective topic. In our work, the locations of the sources are provided by Euler deconvolution. However, this is not a restriction and the interpreter may use any other method. No action was taken.

I don't think it is enough to simply apply your methods to a real data set. To clarify your arguments for the applicability of your methods, you will need to provide more details of this case study. Specifically:

1) include the exploration question that you are trying to answer using your methods;

All geologists want to answer a geologic question. However, many geologic questions are not related to a petroleum exploration question or mining exploration question.

In our manuscript, we want to know the following geological questions. 1) What are the magnetization directions of the alkaline bodies in the study area? 2) Do these bodies belong to the same alkaline province? 3) Were the non-outcropping alkaline bodies emplaced in the subsurface at the same geological time interval?

We have already answered these questions in the manuscript.

2) include the a priori information that allows your methods to be applied, or validate the applicability of your methods here by performing a more thorough investigation of how high you should be upward continuing this real data to safely apply your methods.

We are sorry, but we do not know if we understood your comment.

To validate the result of our Application to field data on the Goiás Alkaline Province, Brazil, we performed a reduction to the pole of the real data. The reduction to the pole was calculated by using the magnetization direction estimated by our method. Notice

Specific comments to the authors:

Line 115:

"This author stresses that ..."

- It is unclear who you are talking about. Please use "We stress that ..." or "Phillips stresses that ...".

Thank you. We have rephrased this sentence.

Line 134:

You may want to point out that the approach taken by Lelievre et al. and Ellis et al. involves a highly nonunique inverse problem and it is critically important to constrain such inversions to reduce the number of acceptable solutions and obtain usable results. This is an important drawback of using such a flexible approach. In contrast, your approach makes heavy assumptions about the underlying sources and is able to reduce the nonuniqueness of the problem to a point that regularization or constraints are not required.

We fully agree with you. We clarified this point in our manuscript.

Line 204:

"In general, the total-field anomaly is produced by a magnetized susceptibility distribution which is anomalous with respect to the mean susceptibility of the crust."

- This statement could be construed to ignore remanent magnetization. It would be more accurate to say something like this: "In general, the total-field anomaly is produced by a

distribution of magnetization which is anomalous with respect to the mean induced magnetization of the crust".

Thank you. We have modified this sentence according to your suggestion.

The forward problem described in section 2.1 is numerically similar to a mesh-based discretization but with the mesh cells (prisms, tetrahedra, etc) replaced with spherical (dipole) sources. What I mean to say is that you have a simple linear multiplication of a full matrix by a vector. Hence, this material could be reduced making use of citations to similar work by other authors.

Thank you for your suggestion. We have decided to maintain the description of the forward problem in section 2.1. Although it is similar to other discretizations presented by other authors, in our opinion, the details described in section 2.1 are extremely important to make our work reproducible.

Line 297:

It would be helpful if you explicitly stated, both here and in the abstract, that you are solving an overdetermined inverse problem, i.e. there are fewer dipole sources than there are data observations, 3L<

Thank you. We have explicitly stated that our method is an overdetermined inverse problem.

Line 361:

You may want to reference the work of Colin Farquharson on general norms here, because he also applied an L1-type measure to the data misfit term and solved iteratively using IRLS.

Farquharson, C.G., and D.W. Oldenburg, 1998. Nonlinear inversion using general measures of data misfit and model structure, Geophysical Journal International, 134, 213-227.

http://webmail2.eos.ubc.ca/sites/default/files/Farquharson_1998.pdf

We agree with you. We added this reference.

<u>Line 365:</u>

"The magnetization vectors are represented in Cartesian coordinates, however they are commonly represented in terms of its intensity, declination and inclination."

- Please provide references in which the magnetization vector is represented by parameters in spherical coordinate systems, and indicate the advantages or disadvantages of such an approach versus using a Cartesian representation.

We are sorry, but we do not know if we understood your comment.

To our knowledge, almost all the classical references in the geophysical literature (and also that ones in our manuscript) represent the magnetization vector in terms of its intensity, declination and inclination.

- Using a spherical framework introduces additional nonlinearity into the problem. How does this affect convergence of the iterative inverse solution? Is convergence guaranteed? Are multiple minima introduced and, if so, are they problematic? Does this suggest that a global optimization strategy should be preferred? Please address these questions in your manuscript.

Thank you for reviewing. The use of a spherical framework would introduce nonlinearity into the problem if the intensity, inclination and declination were the parameters to be estimated. In our method, we estimate the Cartesian coordinates of the vectors h^j (Eq. 12), resulting in a linear inverse problem. We do not solve an iterative nonlinear inverse problem to estimate the intensity, inclination and declination of the magnetization vectors of the sources. We just represent the least-squares and robust estimates in spherical coordinates for convenience, as pointed out in our manuscript. We have introduced some sentences in order to clarify this point.

<u>Section 3.2 Robustness against interfering anomalies.</u>

- I would like to see a test where the assumption of dipole source is still honoured but the two (or more) dipole responses are significantly overlapping. This is what I was expecting when you refer to "interfering anomalies". I think some further research needs to be made into the behaviour of your methods under such a situation.

Thank you for reviewing. We partially agree with your comment. The section 3.2 of our manuscript shows the results obtained by our method in the presence of an interfering anomaly (Fig. 3b) which mostly affect the positive signals of the original total-field anomaly (Fig. 3a). This interference disturbs the dipolar pattern of the original total-field anomaly.

Besides, the total-field anomaly without interference (Fig. 3a) varies from ~ -1550 nT to ~ 750 nT. The total-field anomaly with interference (Fig. 3b) varies from ~ -1550 nT to ~ 1000 nT, showing that the interference represents ~ 33% of the positive amplitude of the original total-field anomaly (Fig. 3a). Therefore, the original total-field anomaly and the interference are significantly overlapping.

However, we recognize that it is possible to formulate a more sophisticated test. Taking this into consideration, we included a new synthetic test showing the results obtained by our method in recovering the magnetization direction of synthetic bodies which simulate a more significantly overlapping anomaly.

See Figure 9 and Table 3 in the new version of the manuscript.

Section 3.4 Robustness against errors in the centre location.

- This is a nice test. However, I'd like to see how well your proposed procedure works here: applying the Euler deconvolution technique to assess the sphere location. Yes, it is of course important to perform the simpler tests with more controls on the variables, but you should also be using the synthetics to demonstrate the behaviour of your proposed procedure for various data characteristics.

Thank you for your suggestion. In light of this, we included a new synthetic test illustrating the performance of our method in recovering the magnetization direction of a more complex source. In this test, we simulated an igneous intrusion formed by a sill which is fed by a vertical pipe. This intrusion is embedded in weakly magnetized sediments that are overlaying a basement which is magnetized by induction, generating a regional anomaly.

See Figures 10-13 and Table 4 in the new version of the manuscript.

What is the location of the sphere calculated through the Euler deconvolution technique and how far is it away from the true location? Please include this information in your manuscript.

Thank you for reviewing. In this subsection, we analyse how the errors in the coordinates of the centre of the source affect the results obtained with our method. The estimated magnetization directions as well as the errors in the location of the source are shown in Figure 7. We did not estimate the location of the sphere through the Euler deconvolution technique because the performance of the Euler deconvolution technique is out of the scope of our work.

Technical corrections:

Please fix the following grammatical errors. There may be others.

Thank you for reviewing. We have fixed all these errors.

Line 25:

"even for other region of the GAP"

Line 27:

"the non-outcropping sources near from the alkaline complex"

Line 28:

"the same magnetization direction of that ones in the alkaline complex"

Line 70:

"and then better defining exploration targets"

Line 105:

"Although this method does not strongly constraint the source's shape"

Line 384:

"are equal to that ones of the magnetization vectors"

On behalf of all authors

Estimation of the total magnetization direction of approximately spherical bodies

V. C. Oliveira Jr.[1]**, D. P. Sales**[1]**, V. C. F. Barbosa**[1]**, and L. Uieda**[1, 2]

[1]Observatório Nacional, Rio de Janeiro, Brazil
[2]Universidade do Estado do Rio de Janeiro, Rio de Janeiro, Brazil

Correspondence to: V. C. Oliveira Jr. (vandscoelho@gmail.com)

Abstract. We have developed a fast total-field anomaly inversion to estimate the magnetization direction of multiple sources with approximately spherical shape and known centres. Our method is an overdetermined inverse problem that
5 can be applied to interpret multiple sources with different but homogeneous magnetization directions. It neither requires the prior computation of any transformation like reduction to the pole nor the use of regularly spaced data on a horizontal grid. The method contains flexibility to be implemented
10 as a linear or non-linear inverse problem, which results, respectively, in a least-squares or robust estimate of the components of the magnetization vector of the sources. Applications to synthetic data show the robustness of our method against interfering anomalies and errors in the location of the
15 sources' centre. Besides, we show the feasibility of applying the upward continuation to interpret non-spherical sources. Applications to field data over the Goiás Alkaline Province (GAP), Brazil, show the good performance of our method in estimating geological meaningful magnetization directions.
20 The results obtained for a region of the GAP, near from the alkaline complex of Diorama, suggest the presence of non-outcropping sources marked by strong remanent magnetization with inclination and declination close to $-70.35°$ and $-19.81°$, respectively. This estimated magnetization di-
25 rection leads to predominantly positive reduced-to-the-pole anomalies, even for other region of the GAP, in the alkaline complex of Montes Claros de Goiás. These results show that the non-outcropping sources near from the alkaline complex of Diorama have almost the same magnetization direction of
30 that as the ones in the alkaline complex of Montes Claros de Goiáás, strongly suggesting that these sources have been emplaced in the crust almost within the same geological time interval.

1 Introduction

The magnetic method is one of the oldest geophysical techniques and plays an important role in mineral and petroleum exploration. This method underwent a great progress after the advent of magnetometers properly developed for airborne surveys. Nowadays, the combination of modern satellite positioning systems and improvements in instrumentation and platform compensation makes the aeromagnetic survey one of the most important data acquisition techniques due to the ability to cover large areas in a relative short period of time (Blakely, 1996; Nabighian et al., 2005). The main applications of the magnetic method are (i) estimating the average depth of the basement relief, (ii) mapping geological faults and abrupt lithological contacts, (iii) defining the limits of mineral targets, (iv) determining the location of geological bodies like salt domes in sediments and (v) identifying geological oil and gas traps. From the physical point of view, all these geological scenarios can be associated to a magnetization distribution produced by magnetized rocks in subsurface. These magnetized rocks are the magnetic sources producing a magnetic induction that can be measured on the Earth's surface or near from it. This magnetic induction causes local differences between the measured data and the magnetic induction predicted by global models describing the geomagnetic field. By isolating these local deviations, the interpreter can determine the magnetic induction produced by the magnetic sources making up the exploration targets.

The total field is the most common magnetic data measured in a survey. It is defined as the Euclidean norm of the magnetic induction produced by all surrounding magnetic sources. After removing the Euclidean norm of the magnetic induction predicted by a global model describing the geomagnetic field and correcting the wide range of undesirable artefacts affecting the data, the result is a scalar quan-

tity denominated total-field anomaly. By using the total-field anomalies, the geophysicist can characterize the magnetic sources in subsurface and then better defining exploration targets (Telford et al., 1990; Blakely, 1996).

Several widely used techniques for interpreting total-field anomalies require the correct knowledge of the magnetization direction of the sources. Among these techniques we emphasize the reduction to pole (Baranov, 1957; Baranov and Naudy, 1964; Silva, 1986), the pseudogravity transformation (Baranov, 1957) and the amplitude of the analytic signal (Nabighian, 1972, 1974, 1984; Li, 2006). Besides, several widely used magnetic inversion methods for estimating the distribution of the magnetization-intensity contrasts in the subsurface also require the knowledge of the correct magnetization direction (Li and Oldenburg, 1996; Pilkington, 1997; Portniaguine and Zhdanov, 1999, 2002; Barbosa and Silva, 2006).

~~Due to the great importance of the~~ Several methods for determining the magnetization direction of the sources have been developed due to its great importance in interpreting total-field anomalies~~, several methods for determining the magnetization direction of the sources have been developed. These methods can be divided~~. Recently, Clark (2014) presented an outstanding and comprehensive review of methods that determine the remanent and total magnetizations of magnetic sources. Here, we present only that ones related to our work.

We divide the methods for retrieving the magnetization direction into two groups. The first one comprises methods that do not impose strong constraints on the shape of the sources. Fedi et al. (1994), for example, accomplished successive RTP's in the wavenumber domain by using different tentative magnetization directions. Among this set of RTP anomalies, these authors choose that one whose amplitude of the negative part is minimum. Since this method uses a wavenumber approach, it requires that the total-field anomaly be regularly spaced in a horizontal grid with constant height to achieve the computational efficiency of the FFT. Besides, it is known that the RTP in the wavenumber domain is unstable at low latitudes and cannot be applied for interpreting total-field anomalies produced by magnetic sources having different magnetization directions. Medeiros and Silva (1995) used the source moments up to second order derived from the multipole expansion of the magnetic potential for estimating the magnetization direction and the spatial orientation of a magnetic source. Although this method does not strongly constraint the source's shape, it presumes that the magnetic source has three orthogonal planes of symmetry intersecting each other at the centre of the source. It is also presumed that the source is far from the observation points. Phillips (2005) proposed a method based on the numerical evaluation of the integrals developed by Helbig (1963) for estimating the magnetization direction and the location of multiple magnetic sources from their first-order magnetic moments. ~~This author~~ Phillips (2005) stresses that

the method is useful for rapid analysis of gridded magnetic data and works best for isolated and compact sources and largely fails for horizontally elongated sources. Tontini and Pedersen (2008) extended this method for using the magnetic moments up to second order to obtain additional information about the horizontal and vertical positions of the centre of the magnetization distribution. Dannemiller and Li (2006) extended the method proposed by Roest and Pilkington (1993), who tackled total-field anomalies produced by generalized 2-D sources, to estimate the magnetization direction of 3-D sources by using the correlation between the vertical gradient and the total gradient of the RTP anomaly obtained through a set of trial directions. These authors stressed that the method assumes that the total-field anomaly is produced by a set of 3-D causative bodies with the same magnetization direction and not by multiple sources with different magnetization directions. A similar method was proposed by Gerovska et al. (2009) based on the comparison between the RTP anomaly and the total magnitude anomaly. Lelièvre and Oldenburg (2009) developed a very flexible method for estimating the magnetization vector distribution in complex geological scenarios. This method discretizes the subsurface of the Earth into a grid of 3-D prisms and estimates the three components (in Cartesian or spherical coordinates) of the magnetization vector of each cell by imposing strong constraints on the solution to deal with the nonuniqueness. Recently, Ellis et al. (2012) presented a similar method to interpret magnetic data in mineral exploration surveys.

The second group of methods to estimate the magnetization direction of the sources assumes the knowledge of the shape of the source. The methods belonging to this group have led to a few published papers. Bhattacharyya (1966), for example, proposed an iterative method for determining the magnetization of a uniformly magnetized rectangular prism. The performance of this method is highly dependent on the correct position of the centre and on the determination of the major and minor axes of the body. Emilia and Massey (1974) developed an iterative method for estimating the vertical magnetization distribution of seamounts. This method approximates the seamounts by vertically juxtaposed right prisms having polygonal horizontal cross sections, which have the same magnetization direction and different magnetization intensities. Parker et al. (1987) also developed a method for estimating the magnetization direction of seamounts. This method was formulated as an optimization problem, named seminorm minimization, to allow estimating a magnetization distribution that is as close as possible to the uniform distribution. However, in practical applications, this constraint may yield a poor data fit. Finally, Kubota and Uchiyama (2005) discretized the seamount volume as a grid of juxtaposed right rectangular prisms and estimated the Cartesian components of the magnetization vector of each prism.

In this work, we present a computationally efficient method for inverting the total-field anomaly produced by

multiple sources with approximately spherical shape to estimate their magnetization directions. We assume sources with known centre, which can be provided by Euler deconvolution, for example. The proposed method is part of the group of methods imposing assumptions about the shape of the magnetic sources. ~~It~~ This assumptions about the underlying sources is able to reduce the nonuniqueness of the problem to a point that regularization or constraints are not required. Our method can be applied for ~~interpreting multiple sourceswith different magnetization directions. It does not require the~~ estimating the average magnetization direction of multiple sources. It neither requires that all sources have the same magnetization direction nor the use of regularly spaced data on a horizontal grid~~and~~. Besides, our method also contains flexibility to be implemented in two different numerical approaches. The first one minimizes an L2-norm, resulting in a linear inverse problem to obtain a least-squares estimate. The second approach comprises the iterative minimization of an L1-norm, resulting in a non-linear inverse problem to obtain a robust estimate. Applications to synthetic data show the robustness of our method against interfering anomalies and errors in the location of the sources' centre. Additionally, we show how the upward continuation can be used to make possible the application of our method to interpret non-spherical sources. Applications to field data over the Goiás Alkaline Province (GAP), Brazil, show the good performance of the proposed method in estimating geological meaningful magnetization directions. The obtained results over a region of the GAP, near from the alkaline complex of Diorama, suggest the presence of non-outcropping sources with strong remanent magnetization, corroborating previous works. The estimated inclinations and declinations are close to $-70.35°$ and $-19.81°$, respectively.

2 Methodology

2.1 Parameterization and forward problem

Let $\boldsymbol{\Delta T}^{\mathrm{o}}$ be the observed data vector, whose ith element ΔT_i^{o}, $i = 1, \ldots, N$, is the total-field anomaly measured at the position (x_i, y_i, z_i) (black dots in Fig. 1). In this Cartesian coordinate system, x points to the geographic north, y points to east and z points downward. In general, the total-field anomaly is produced by a ~~magnetized susceptibility distribution~~ distribution of magnetization which is anomalous with respect to the mean ~~susceptibility~~ induced magnetization of the crust. Mathematically, ΔT_i^{o} can be written as

$$\Delta T_i^{\mathrm{o}} = \|\boldsymbol{T}_i\| - \|\boldsymbol{F}_i\|, \tag{1}$$

where $\|\cdot\|$ indicates the Euclidean norm, $\boldsymbol{F}_i$ is the geomagnetic field vector and $\boldsymbol{T}_i$ is the total-field vector, both at (x_i, y_i, z_i). The total-field vector can be represented by the sum

$$\boldsymbol{T}_i = \boldsymbol{F}_i + \boldsymbol{B}_i, \tag{2}$$

where $\boldsymbol{B}_i$ is the total magnetic induction vector produced by all magnetic sources (magnetized anomalous susceptibility distribution) at the position (x_i, y_i, z_i) (Blakely, 1996; Langel and Hinze, 1998).

For local or regional scale magnetic studies, it is very common to consider that (i) the geomagnetic field $\boldsymbol{F}_i$ (Eq. 1) is a constant vector $\boldsymbol{F}_0$ throughout the study area and (ii) that $\|\boldsymbol{F}_0\| \gg \|\boldsymbol{B}_i\|$, $i = 1, \ldots, N$ (Telford et al., 1990; Blakely, 1996). The second assumption is equivalent to say that the total magnetic induction $\boldsymbol{B}_i$ (Eq. 1) is a small perturbation of the geomagnetic field $\boldsymbol{F}_i$ throughout the study area. These two assumptions make possible to approximate the Euclidean norm of the total-field vector $\boldsymbol{T}_i$ (Eq. 1) by a first-order Taylor's expansion as follows

$$
\begin{aligned}
\|\boldsymbol{T}_i\| &\approx \|\boldsymbol{F}_0 + \boldsymbol{B}_i\| \\
&\approx \|\boldsymbol{F}_0\| + \hat{\boldsymbol{F}}^{\mathrm{T}} \boldsymbol{B}_i,
\end{aligned}
\tag{3}
$$

where the superscript T indicates transposition and

$$\hat{\boldsymbol{F}} = \frac{\boldsymbol{F}_0}{\|\boldsymbol{F}_0\|} \tag{4}$$

is a unit vector (with the same direction of the geomagnetic field $\boldsymbol{F}_i$) representing the gradient of the function $\|\boldsymbol{T}_i\|$ with respect to the components of the vector $\boldsymbol{T}_i$ (Blakely, 1996). By introducing this first-order Taylor's expansion into the total-field anomaly (Eq. 1), we obtain the well-known approximated total-field anomaly given by

$$\Delta T_i \approx \hat{\boldsymbol{F}}^{\mathrm{T}} \boldsymbol{B}_i, \qquad i = 1, \ldots, N. \tag{5}$$

Let's consider that the magnetic sources can be represented by a set of L uniformly magnetized spheres. In this case, the total magnetic induction $\boldsymbol{B}_i$ is given by

$$\boldsymbol{B}_i = \sum_{j=1}^{L} \boldsymbol{b}_i^j, \qquad i = 1, \ldots, N, \tag{6}$$

being $\boldsymbol{b}_i^j$ the magnetic induction produced, at the position (x_i, y_i, z_i), by the jth sphere, $j = 1, \ldots, L$, with radius R_j (dashed straight lines in Fig. 1), centre at (xc_j, yc_j, zc_j) (grey dots in Fig. 1) and magnetization vector $\boldsymbol{m}^j$ given by

$$\boldsymbol{m}^j = \begin{bmatrix} mx_j \\ my_j \\ mz_j \end{bmatrix}_{3 \times 1}. \tag{7}$$

The magnetic induction $\boldsymbol{b}_i^j$ (Eq. 6) can be written as

$$\boldsymbol{b}_i^j = C_m \mathbf{M}_i^j \frac{4}{3} \pi R_j^3 \boldsymbol{m}^j, \tag{8}$$

where C_m is a constant given by $\mu_0 / 4\pi = 10^{-7}\ H/m$, μ_0 is the vacuum permeability and $\mathbf{M}_i^j$ is the matrix

$$\mathbf{M}_i^j = \begin{bmatrix} \left(\frac{\partial^2}{\partial x \partial x} \frac{1}{r_j}\right) & \left(\frac{\partial^2}{\partial x \partial y} \frac{1}{r_j}\right) & \left(\frac{\partial^2}{\partial x \partial z} \frac{1}{r_j}\right) \\ \left(\frac{\partial^2}{\partial x \partial y} \frac{1}{r_j}\right) & \left(\frac{\partial^2}{\partial y \partial y} \frac{1}{r_j}\right) & \left(\frac{\partial^2}{\partial y \partial z} \frac{1}{r_j}\right) \\ \left(\frac{\partial^2}{\partial x \partial z} \frac{1}{r_j}\right) & \left(\frac{\partial^2}{\partial y \partial z} \frac{1}{r_j}\right) & \left(\frac{\partial^2}{\partial z \partial z} \frac{1}{r_j}\right) \end{bmatrix}_{3 \times 3}, \tag{9}$$

whose elements are the second derivatives, evaluated at the position (x_i, y_i, z_i), of the function

$$\frac{1}{r_j} \equiv \frac{1}{\sqrt{(x - xc_j)^2 + (y - yc_j)^2 + (z - zc_j)^2}} \quad (10)$$

with respect to the variables x, y and z. By substituting the magnetic induction $\boldsymbol{b}_i^j$ (Eq. 8) into the total magnetic induction vector $\boldsymbol{B}_i$ (Eq. 6) and using the approximated total-field anomaly (Eq. 5) we obtain the predicted total-field anomaly d_i produced by the set of L spheres at the position (x_i, y_i, z_i) as follows

$$d_i = \hat{\boldsymbol{F}}^{\mathrm{T}} \sum_{j=1}^{L} \mathbf{M}_i^j \boldsymbol{h}^j, \quad (11)$$

where

$$\boldsymbol{h}^j = C_m \frac{4}{3} \pi R_j^3 \boldsymbol{m}^j, \qquad j = 1, \ldots, L. \quad (12)$$

This equation shows that each vector $\boldsymbol{h}^j$ has the same direction of the magnetization vector $\boldsymbol{m}^j$, $j = 1, \ldots, L$ (Eq. 7). In Cartesian coordinates, we have $\boldsymbol{h}^j = [hx_j\, hy_j\, hz_j]^{\mathrm{T}}$ (Fig. 2), where $h\alpha_j = C_m \frac{4}{3} \pi R_j^3 m\alpha_j$, $\alpha = x, y, z$, $j = 1, \ldots, L$, and $m\alpha_j$, $\alpha = x, y, z$, are the elements of the magnetization vector $\boldsymbol{m}^j$ (Eq. 7). Equation (11) can be rewritten as

$$d_i(\boldsymbol{h}) = \boldsymbol{a}_i^{\mathrm{T}} \boldsymbol{h}, \quad (13)$$

where

$$\boldsymbol{h} = \begin{bmatrix} \boldsymbol{h}^1 \\ \vdots \\ \boldsymbol{h}^L \end{bmatrix}_{3L \times 1}, \quad (14)$$

and

$$\boldsymbol{a}_i = \begin{bmatrix} \mathbf{M}_i^1 \hat{\boldsymbol{F}} \\ \vdots \\ \mathbf{M}_i^L \hat{\boldsymbol{F}} \end{bmatrix}_{3L \times 1}. \quad (15)$$

Note that, in Eq. (13), the predicted total-field anomaly d_i (Eq. 11) is represented by $d_i(\boldsymbol{h})$ in order to express its dependence on the parameter vector $\boldsymbol{h}$ (Eq. 14). The linear relationship given by Eq. (13) can be written in matrix notation as

$$\boldsymbol{d}(\boldsymbol{h}) = \mathbf{A}\boldsymbol{h}, \quad (16)$$

where $\boldsymbol{d}(\boldsymbol{h})$ is the N-dimensional predicted data vector, whose ith element is $d_i(\boldsymbol{h})$ (Eq. 13), and $\mathbf{A}$ is a $N \times 3L$ matrix $(N > 3L)$ that can be partitioned as

$$\mathbf{A} = \begin{bmatrix} \boldsymbol{a}_1^{\mathrm{T}} \\ \vdots \\ \boldsymbol{a}_N^{\mathrm{T}} \end{bmatrix}_{N \times 3L}, \quad (17)$$

being $\boldsymbol{a}_i$, $i = 1, \ldots, N$, the $3L$-dimensional vector defined in Eq. (15).

2.2 Inverse problem

We assume that the magnetic sources giving rise to the observed data $\boldsymbol{\Delta T}^{\mathrm{o}}$ can be approximated by a set of L uniformly magnetized spheres with known coordinates (xc_j, yc_j, zc_j), $j = 1, \ldots, L$, of their centres. We also assume that the direction of the constant geomagnetic field $\boldsymbol{F}_0$ (Eq. 4) is known. Under these hypotheses, we formulate ~~a~~ an overdetermined linear inverse problem of estimating the parameter vector $\boldsymbol{h}$ (Eq. 14) from $\boldsymbol{\Delta T}^{\mathrm{o}}$. The problem of estimating a parameter vector $\boldsymbol{h}$ (Eq. 14) containing the magnetization vectors $\boldsymbol{m}^j$ (Eq. 7), $j = 1, \ldots, L$, of the L spheres can be done by minimizing the goal function

$$\Psi(\boldsymbol{h}) = \frac{1}{N} [\boldsymbol{\Delta T}^{\mathrm{o}} - \boldsymbol{d}(\boldsymbol{h})]^{\mathrm{T}} [\boldsymbol{\Delta T}^{\mathrm{o}} - \boldsymbol{d}(\boldsymbol{h})]. \quad (18)$$

Differentiating Eq. (18) with respect to $\boldsymbol{h}$ and equating the result to the null vector, we obtain the normal equation for the least-squares estimate $\hat{\boldsymbol{h}}$, i. e.,

$$(\mathbf{A}^{\mathrm{T}}\mathbf{A})\hat{\boldsymbol{h}} = \mathbf{A}^{\mathrm{T}} \boldsymbol{\Delta T}^{\mathrm{o}}. \quad (19)$$

The least-squares estimate $\hat{\boldsymbol{h}}$ (Eq. 19) minimizes the goal function (Eq. 18) and produces the predicted data $\boldsymbol{d}(\hat{\boldsymbol{h}})$ (Eq. 16) as near as possible from the observed data $\boldsymbol{\Delta T}^{\mathrm{o}}$, in the L2-norm sense (Bard, 1973; Twomey, 1977; Menke, 1989; Aster et al., 2005).

The least-squares estimate $\hat{\boldsymbol{h}}$ (Eq. 19) is very sensitive to outliers in the observed data. In some cases, if the outliers are not properly removed from the observed data, the estimated parameters can be seriously misleading. When working with field data, the outliers can be caused by interfering magnetic sources or cultural noise, for example. To counteract this problem automatically, we can use a robust scheme for minimizing the goal function

$$\Gamma(\boldsymbol{h}) = \frac{1}{N} \sum_{i=1}^{N} |\Delta T_i^{\mathrm{o}} - d_i(\boldsymbol{h})|. \quad (20)$$

Different from Eq. (18), the parameter vector $\boldsymbol{h}$ minimizing the Eq. (20) cannot be obtained by solving a linear system. One practical way is the Iteratively Reweighted Least Squares algorithm ~~(Scales et al., 1988; Aster et al., 2005)~~ (Scales et al., 1988; Farquharson In this algorithm, at each iteration k, the following linear system is solved:

$$(\mathbf{A}^{\mathrm{T}}\mathbf{R}^k\mathbf{A})\tilde{\boldsymbol{h}}^{k+1} = \mathbf{A}^{\mathrm{T}}\mathbf{R}^k \boldsymbol{\Delta T}^{\mathrm{o}}, \quad (21)$$

where $\mathbf{R}^k$ is a diagonal $N \times N$ matrix whose ith element r_i^k, $i = 1, \ldots, N$, is given by

$$r_i^k = \frac{1}{\left| \Delta T_i^{\mathrm{o}} - d_i\left(\tilde{\boldsymbol{h}}^k\right) + \epsilon \right|}, \quad (22)$$

being ϵ a small positive number used to prevent singularities. This iterative process begins (iteration $k = 0$) with the least-squares estimate $\tilde{h}^0 = \hat{h}$ (Eq. 19). With this initial approximation $\tilde{h}^0$, we calculate the matrix $\mathbf{R}^0$ (Eq. 22). By using the matrix $\mathbf{R}^0$, we solve the linear system given by Eq. (21) for obtaining the estimate $\tilde{h}^1$. By using the updated estimate $\tilde{h}^1$, we calculate the matrix $\mathbf{R}^1$ (Eq. 22), solve the linear system (Eq. 21) for obtaining the updated estimate $\tilde{h}^2$ and so on. After some iterations, this iterative procedure converges to the estimate $\tilde{h}$, which is named robust estimate and is an approximation of the parameter vector minimizing the function $\Gamma(h)$ (Eq. 20).

Both $\hat{h}$ (least-squares estimate) and $\tilde{h}$ (robust estimate) are estimates of the ~~Cartesian coordinates of the~~ parameter vector h (Eq. 14), which is represented as a function of the vectors h^j, $j = 1, \ldots, L$ (Eq. 12) and the magnetization vectors m^j, $j = 1, \ldots, L$ (Eq. 7). ~~The~~ However, magnetization vectors are ~~represented in Cartesian coordinates, however they are~~ commonly represented in terms of its intensity, declination and inclination. Therefore, for convenience, we will represent the vectors h^j (Eq. 12) in spherical coordinates as follows

$$h^j = Q_j \begin{bmatrix} \cos I_j \cos D_j \\ \cos I_j \sin D_j \\ \sin I_j \end{bmatrix}_{3 \times 1}, \qquad (23)$$

where the intensity Q_j, declination D_j and inclination I_j are given as functions of the elements hx_j, hy_j and hz_j (Fig. 2) of h^j, i.e.,

$$Q_j = \sqrt{hx_j^2 + hy_j^2 + hz_j^2}, \qquad (24)$$

$$D_j = \arctan\left(\frac{hy_j}{hx_j}\right), \qquad (25)$$

and

$$I_j = \arctan\left(\frac{hz_j}{\sqrt{hx_j^2 + hy_j^2}}\right). \qquad (26)$$

Note that, according to Eq. (12), the declinations D_j (Eq. 25) and inclinations I_j (Eq. 26), $j = 1, \ldots, L$, are equal to that ones of the magnetization vectors m^j, $j = 1, \ldots, L$ (Eq. 7). After obtaining the least-squares estimate $\hat{h}$ or the robust estimate $\tilde{h}$ in Cartesian coordinates, we calculate the declinations $\hat{D}_j$ or $\tilde{D}_j$ (Eq. 25) and inclinations $\hat{I}_j$ or $\tilde{I}_j$ (Eq. 26), $j = 1, \ldots, L$, of the total magnetization vector of all spheres. We use a caret ($\hat{\ }$) and a tilde ($\tilde{\ }$) to distinguish estimates of the declinations and inclinations which are computed by using, respectively, the least-square estimate $\hat{h}$ and the robust estimate $\tilde{h}$.

2.3 Uncertainty of the estimated parameters

In a magnetic survey, the measurements are always affected by noise due to the wide range of experimental errors and inaccuracies that happens in a geophysical survey. The noise in the observed data ΔT^o affects the estimated parameter vector, independently of the used method. To quantify this effect on the estimated parameters, we can use the propagation of covariance (Bard, 1973; Aster et al., 2005). By presuming that the errors of all observed data ΔT_i^o, $i = 1, \ldots, N$, are independent and of equal variance σ^2, we obtain the data covariance matrix $\mathbf{D} = \sigma^2 \mathbf{I}$, where $\mathbf{I}$ is the $N \times N$ identity matrix. The parameter covariance matrix $\hat{\mathbf{C}}$ of the least-squares estimate $\hat{h}$ (Eq. 19) is given by

$$\hat{\mathbf{C}} = \hat{\mathbf{H}}\mathbf{D}\hat{\mathbf{H}}^T, \qquad (27)$$

where

$$\hat{\mathbf{H}} = (\mathbf{A}^T\mathbf{A})^{-1}\mathbf{A}^T. \qquad (28)$$

Similarly, the parameter covariance matrix $\tilde{\mathbf{C}}$ of the robust estimate $\tilde{h}$ (Eqs. 21 and 22) can be given by

$$\tilde{\mathbf{C}} = \tilde{\mathbf{H}}\mathbf{D}\tilde{\mathbf{H}}^T, \qquad (29)$$

where

$$\tilde{\mathbf{H}} = (\mathbf{A}^T\mathbf{R}^k\mathbf{A})^{-1}\mathbf{A}^T\mathbf{R}^k, \qquad (30)$$

and the matrix $\mathbf{R}^k$ (Eq. 21) is the last one calculated in the iterative process for estimating $\tilde{h}$ (Bard, 1973; Aster et al., 2005).

The diagonal of the parameter covariance matrices $\hat{\mathbf{C}}$ (Eq. 27) and $\tilde{\mathbf{C}}$ (Eq. 29) contains the variances of the elements of the estimates $\hat{h}$ (Eq. 19) and $\tilde{h}$ (Eqs. 21 and 22), respectively. Let v be a $3L$-dimensional vector whose element v_j, $j = 1, \ldots, 3L$, represents the jth element of the diagonal of the covariance matrix $\hat{\mathbf{C}}$ (Eq. 27) or $\tilde{\mathbf{C}}$ (Eq. 29). This vector can be represented by

$$v = \begin{bmatrix} v^1 \\ \vdots \\ v^L \end{bmatrix}_{3L \times 1}, \qquad (31)$$

where

$$v^j = \begin{bmatrix} (\sigma x_j)^2 \\ (\sigma y_j)^2 \\ (\sigma z_j)^2 \end{bmatrix}_{3 \times 1}, \qquad (32)$$

and $\sigma\alpha_j$, $\alpha = x, y, z$, $j = 1, \ldots, L$, are the uncertainties of the components $h\alpha_j$, $\alpha = x, y, z$, $j = 1, \ldots, L$, of the vectors h^j, $j = 1, \ldots, L$ (Eq. 12), forming the estimated parameter vector $\hat{h}$ or $\tilde{h}$. The uncertainties of the intensity Q_j, declination D_j and inclination I_j can be given as functions of the uncertainties $\sigma\alpha_j$, $\alpha = x, y, z$, $j = 1, \ldots, L$ (Eq. 32). To do it, we use the propagation of uncertainties (Fornasini, 2008) and presume that the components $h\alpha_j$, $\alpha = x, y, z$, $j = 1, \ldots, L$, of the vector h^j (Eq. 12) are statistically independent. From

this assumption, the uncertainties σ_{Qj}, σ_{Dj} and σ_{Ij} of the intensity Q_j (Eq. 24), declination D_j (Eq. 25) and inclination I_j (Eq. 26) are respectively given by

$$\sigma_{Qj} = \sqrt{\left(\frac{\partial Q_j}{\partial hx_j}\sigma x_j\right)^2 + \left(\frac{\partial Q_j}{\partial hy_j}\sigma y_j\right)^2 + \left(\frac{\partial Q_j}{\partial hz_j}\sigma z_j\right)^2}, \tag{33}$$

$$\sigma_{Dj} = \sqrt{\left(\frac{\partial D_j}{\partial hx_j}\sigma x_j\right)^2 + \left(\frac{\partial D_j}{\partial hy_j}\sigma y_j\right)^2} \tag{34}$$

and

$$\sigma_{Ij} = \sqrt{\left(\frac{\partial I_j}{\partial hx_j}\sigma x_j\right)^2 + \left(\frac{\partial I_j}{\partial hy_j}\sigma y_j\right)^2 + \left(\frac{\partial I_j}{\partial hz_j}\sigma z_j\right)^2}. \tag{35}$$

The first-order derivatives shown in Eqs. (33), (34) and (35) are given by

$$\frac{\partial Q_j}{\partial h\alpha_j} = \frac{h\alpha_j}{Q_j}, \alpha = x, y, z, \tag{36}$$

$$\frac{\partial D_j}{\partial hx_j} = \frac{-hy_j}{(hx_j)^2 + (hy_j)^2}, \tag{37}$$

$$\frac{\partial D_j}{\partial hy_j} = \frac{hx_j}{(hx_j)^2 + (hy_j)^2}, \tag{38}$$

$$\frac{\partial I_j}{\partial h\alpha_j} = \frac{-h\alpha_j hz_j}{Q_j^2\sqrt{(hx_j)^2 + (hy_j)^2}}, \alpha = x, y, \tag{39}$$

and

$$\frac{\partial I_j}{\partial hz_j} = \frac{\sqrt{(hx_j)^2 + (hy_j)^2}}{Q_j^2}. \tag{40}$$

We use a caret ($\,\hat{}\,$) and a tilde ($\,\tilde{}\,$) to distinguish the uncertainties ($\hat{\sigma}$ and $\tilde{\sigma}$) computed by using, respectively, the least-squares $\hat{h}$ and the robust $\tilde{h}$ estimates.

2.4 Software implementation

The inversion method described above is implemented in version 0.3 of the open-source Python language library Fatiando a Terra[12]. We used *matplotlib* (Hunter, 2007) for graphs and maps and *Mayavi* (Ramachandran and Varoquaux, 2011) for 3D figures. The results and figures from the application to synthetic and real data were produced in IPython notebooks (Pérez and Granger, 2007). The notebooks contain explanatory text as well as the source code used to generate the synthetic data, run the inversions, and produce figures. The IPython notebooks and instructions for installing the required software and reproducing our results are available as online supplementary material[34].

[1] http://www.fatiando.org/
[2] http://dx.doi.org/10.5281/zenodo.16205
[3] https://github.com/pinga-lab/Total-magnetization-of-spherical-bodies
[4] http://dx.doi.org/10.5281/zenodo.16191

3 Application to synthetic data

3.1 Validation test

Figure 3a shows the synthetic noise-corrupted total-field anomaly produced by two uniformly magnetized bodies embedded in nonmagnetic host rocks. The first one is a sphere with radius $1000\,\text{m}$, centre at $xc = 3000\,\text{m}$, $yc = 3000\,\text{m}$, $zc = 1000\,\text{m}$ and magnetization vector with intensity $6\,\text{A}\,\text{m}^{-1}$, declination $10°$ and inclination $20°$. The second synthetic body is a rectangular prism with horizontal and vertical dimensions equal to $1000\,\text{m}$, depth of the top at $200\,\text{m}$, centre at $xc = 7000\,\text{m}$, $yc = 7000\,\text{m}$, $zc = 700\,\text{m}$ and magnetization vector with intensity $6\,\text{A}\,\text{m}^{-1}$, declination $40°$ and inclination $30°$. We simulated a constant geomagnetic field $\boldsymbol{F}^\circ$ (Eq. 3) with declination $15°$ and inclination $10°$. The total field anomaly produced by these synthetic bodies (indicated by A and B in Fig. 3) was calculated at $N = 10\,000$ irregularly spaced points (x_i, y_i, z_i), $i = 1, \ldots, N$, on the plane with constant vertical coordinate $z = -150\,\text{m}$, extending from 0 to $10\,000\,\text{m}$ in both x and y directions. The pseudorandom Gaussian noise added has a zero mean and a standard deviation of $5\,\text{nT}$.

By assigning the correct positions of the centres of the simulated bodies, we invert the noise-corrupted total-field anomaly (Fig. 3a) to obtain the least-squares estimate $\hat{\boldsymbol{h}}$ (Eq. 19) and robust estimate $\tilde{\boldsymbol{h}}$ (Eqs. 21 and 22). Next, we use these estimates to calculate the estimated declinations and inclinations (Eqs. 25 and 26). Finally, we calculate the uncertainties using the propagation of covariance (Eqs. 27–30) and assuming that the standard deviation of the errors is equal to the true one ($\sigma = 5\,\text{nT}$). The results (Table 1) show that our method is able to retrieve the magnetization directions of the true sources by using either the least-squares or robust estimate. Even in the case of the prism that violates the premise assumed by our method that the bodies can be approximated by spheres, the estimates are very close to the true ones with a small uncertainties. We can attribute this good performance of our method to three factors: (i) the absence of interfering signals produced, for example, by multiple magnetic sources, (ii) the simulated prism is a cube that seems a sphere-like body; and (iii) the use of the correct locations of the centres of the simulated bodies. The following tests will show how these factors affect the results obtained by using the least-squares and robust estimates.

3.2 Robustness against interfering anomalies

Figure 3b shows the noise-corrupted total-field anomaly shown in Fig. 3a contaminated with interfering anomalies. These interfering anomalies are characterized by midwavelength components which mostly affect the positive signals of the original total-field anomaly (Fig. 3a), resulting in non-dipolar total-field anomalies (Fig. 3b). The interfering anomalies reach approximately 33% of the

positive amplitude of the original total-field anomaly shown in Fig. 3a. Notice that this test violates the premise assumed by our method that the total-field anomalies are caused by dipolar bodies (spheres). Although these interfering anomalies are different from random Gaussian noise or outliers marked as spurious errors dominated by short-wavelength spectral contents, they can also be seen as a data noise.

We repeated the numerical test presented in the previous section (Sect. 3.1), but using the contaminated total-field anomaly shown in Fig. 3b. The results are shown in Table 2. As we can see, the results obtained with the least-squares estimate are very affected by the interfering anomalies if compared with that ones obtained by using the robust estimate. By comparing the true values of inclination I and declination D with that ones obtained with the least-squares estimate, the differences reach approximately $14°$ in declination and $9°$ in inclination. On the other hand, the differences between the results obtained with the robust estimate and the true values reach only $2°$ in declination and $3°$ in inclination. These results suggest that the least-squares estimate is more sensitive to interfering anomalies than the robust estimate.

3.3   Robustness against non-spherical sources

In the previous subsections, we applied our method to estimate the magnetization direction of a rectangular prism whose total-field anomaly is indicated by B in Fig. 3. This total-field anomaly is similar to one that would be produced by a sphere. Two factors contribute to this: (i) the prism has all edges equal to $1000\,\mathrm{m}$ and (ii) the distance between its top depth and the plane surface on which the data were calculated is $350\,\mathrm{m}$. In this subsection, we analyse the effect of these two factors on the results obtained with our method. To do it, we applied our method to estimate the magnetization direction of 11 rectangular prisms with different side lengths Lx, Ly and Lz (Fig. 4a) and top at $10\,\mathrm{m}$ deep. All prisms have uniform magnetization with intensity, declination and inclination equal to $6\,\mathrm{A\,m^{-1}}$, $-40°$ and $30°$, respectively, centre at $xc = 0\,\mathrm{m}$, $yc = 0\,\mathrm{m}$ and $zc = 510\,\mathrm{m}$ and side lengths $Lx = Lz = 1000\,\mathrm{m}$. For simplicity, we adopted dimensionless quantities by normalizing all coordinates and lengths by the numerical value of Lz ($1000\,\mathrm{m}$), implying that $Lx = Lz = 1.0$. The only difference between these 11 prisms is the side length Ly, which varies regularly from 0.2 to 1.8. Figure 4b shows the x–y cross-section of three different rectangular prisms with Ly equal to 0.2, 1.0 and 1.8. We calculated the noise-corrupted total-field anomalies produced by all prisms on horizontal planes with constant z equal to 0.0, -0.3 and -0.6 (dashed lines in Fig. 4b), resulting in 33 synthetic data sets. All data are calculated at $N = 3000$ points irregularly spaced over an area extending from -5 to 5 along the x and y directions. The pseudo-random Gaussian noise added has a zero mean and a standard deviation of 5 nT. The simulated constant geomagnetic field $\boldsymbol{F}_0$ (Eq. 3) has declination $-15°$ and inclination $-10°$.

Figure 5a–c show that total-field anomalies calculated near from the sources are very different to that ones produced by spherical bodies (dipolar sources) and exhibit strongly non-dipolar features. These non-dipolar features are attenuated if the data are calculated far from the sources (Fig. 5g–i), showing the well known property that the magnetic field produced by a non-dipolar source tends to the field produced by a dipolar source at great distances. This attenuation is more noticeable for sources presenting symmetry around three orthogonal axis. This higher attenuation for symmetrical sources can be seen by comparing Fig. 5b, e and h, which show anomalies produced by a cube with $Lx = Ly = Lz = 1.0$, with Fig. 5a, c, d, f, g and i, which show anomalies produced by other rectangular prisms. For example, on the plane $z = -0.3$, the total-field anomaly produced by the cube (Fig. 5h) displays approximately a dipolar feature while the total-field anomalies produced by the other prisms (Fig. 5d and f) exhibit non-dipolar features.

We applied our method to interpret these 33 data sets and the results are shown in Fig. 6. In all these applications, we presume the correct location of the centre of the sources. Figure 6 shows that the robust estimates (red dots) are much better than the least-squares estimates (blue dots). This better performance is noteworthy for the estimated declinations obtained by inverting the total-field anomalies near from the sources (red dots in Fig. 6a). The least-squares estimates (blue dots in Fig. 6a and b) seem to be more sensitive to the strong non-dipolar total-field anomalies (e.g., Fig. 5a–c). By inverting the total-field anomalies far the sources (e.g., Fig. 5d–i), the least-squares estimates are approximately similar to the robust estimates (Fig. 6c–f).

The greater the distance between the sources and the data, the greater the attenuation of the non-dipolar features; and thus the smaller the difference between the least-squares and robust estimates. In this case, a good practice when applying our method is to perform an upward continuation of the total-field anomaly to be inverted.

3.4   Robustness against errors in the centre location

In all previous tests with synthetic data, we presume the correct location of the centre of the sources. However, in real world scenarios, the position of the sources cannot be obtained directly and have to be estimated. This estimation can be done, for example, by using the Euler deconvolution technique (Thompson, 1982; Reid et al., 1990). This is a classical technique to estimate the 3-D position of magnetic sources (Reid et al., 2014; Ueda et al., 2014). Like all numerical techniques, the estimates obtained via Euler deconvolution contain errors that will affect the results obtained with our method. So, in this subsection, we analyse how the errors in the coordinates of the centre of the source affect the results obtained with our method.

We simulated a uniformly magnetized sphere (not shown) with centre at $xc = 5000\,\mathrm{m}$, $yc = 5000\,\mathrm{m}$ and $zc = 1000\,\mathrm{m}$,

radius $R = 1000\,\mathrm{m}$ and magnetization vector with intensity $8.0\,\mathrm{A\,m^{-1}}$, declination $-13°$ and inclination $-40°$. The simulated constant geomagnetic field $\boldsymbol{F}_0$ (Eq. 3) has declination $-13°$ and inclination $-9.5°$. The noise-corrupted total-field anomaly (not shown) produced by this sphere is calculated at $N = 2601$ points equally spaced on a plane with constant $z = -150\,\mathrm{m}$, extending from $0\,\mathrm{m}$ to $10\,000\,\mathrm{m}$ along both the x and y axis. The pseudo-random Gaussian noise added has null mean and standard deviation equal to 2 nT.

We applied our method to this synthetic data for estimating the magnetization direction of the simulated spherical body. This application was done by presuming different locations of the centre of the source along three orthogonal straight lines which are parallel to the x, y and z axis and cross the centre of the simulated spherical body. Along each line, we varied the centre of the source at 21 points regularly spaced in a range of $2000\,\mathrm{m}$. The results obtained along the x, y and z axis are shown in Fig. 7a–f, respectively.

We can clearly see that the wrong choice of the x and y coordinates of the center of the source leads to poor estimates of the magnetization direction (declinations and inclinations in Fig. 7a–d) when compared with the true magnetization vector (continuous black lines in Fig. 7). On the other hand, the estimated declinations and inclinations are less sensitive to the wrong choice of the z coordinate of the centre of the source (Fig. 7e and f), especially the ones obtained by the least-squares estimate. These results show that our method is more sensitive to uncertainties in the prior information about location of the centre of the source along the horizontal directions than in the vertical direction. Fortunately, the sensitivity of Euler deconvolution to estimate the 3-D position of magnetic sources works in opposite direction. As shown by Silva and Barbosa (2003) and Melo et al. (2013), the estimates of the source horizontal positions in Euler deconvolution are very accurate while the depth estimates may fail. This characteristic makes Euler deconvolution a suitable technique for providing the centre of the source to be used by our method as prior information to form the matrix given in Eq. (17).

3.5 Complex tests

In this section, we present the performance of our method in recovering the magnetization direction of synthetic sources simulating complex geological scenarios.

3.5.1 Strong-interfering anomalies

Figure 8 shows two synthetic sources simulating uniformly magnetized bodies embedded in nonmagnetic host rocks. Both sources are rectangular prisms with horizontal dimensions equal to $80\,\mathrm{m}$ and $20\,\mathrm{m}$ along the x and y directions, respectively, vertical dimension equal to $70\,\mathrm{m}$ and depth of the top at $z = 10\,\mathrm{m}$ (red prisms in Fig. 8). One source has its centre at $xc = 0\,\mathrm{m}$, $yc = -30\,\mathrm{m}$ and $zc = 45\,\mathrm{m}$ while the other one has its centre shifted $60\,\mathrm{m}$ in the positive y direction (pinpointed black dots in Fig. 8). Both sources have a Koenigsberger ratio equal to 3 and the same induced magnetization with intensity $3\,\mathrm{A\,m^{-1}}$, declination $0°$ and inclination $-30°$. The remanent magnetization of the sources has the same inclination equal to $0°$, but different declinations equal to $30°$ (eastern source) and $-30°$ (western source). The total field anomaly produced by these synthetic bodies (Fig. 9) was calculated at $N = 2601$ regularly spaced points (x_i, y_i, z_i), $i = 1, \ldots, N$, on the plane with constant vertical coordinate $z = -10\,\mathrm{m}$, extending from -200 to 200 m in both x and y directions. The pseudorandom Gaussian noise added has a zero mean and a standard deviation equal to 2% of the peak-to-peak amplitude of the noise-free total-field anomaly. This synthetic test was inspired by a test shown in Lelièvre and Oldenburg (2009) .

By assigning the correct positions of the centres of the simulated bodies, we invert the noise-corrupted total-field anomaly (Fig. 9) to obtain the least-squares estimate $\hat{\boldsymbol{h}}$ (Eq. 19) and robust estimate $\tilde{\boldsymbol{h}}$ (Eqs. 21 and 22). Next, we use these estimates to calculate the estimated declinations and inclinations (Eqs. 25 and 26). Finally, we calculate the uncertainties using the propagation of covariance (Eqs. 27–30) by assuming that the standard deviation of the errors is equal to the true one. The results (Table 3) show the good performance of our method in estimating the magnetization directions of non-spherical sources producing strong-interfering anomalies. This test also shows the better performance of the robust estimate as compared with the least-squares estimate.

3.5.2 Igneous intrusion within a sedimentary basin

Figure 10 shows a 2D schematic representation of a synthetic geological setting where an igneous intrusion (red prisms) is embedded in a nonmagetic sedimentary pack (grey area). The igneous intrusion is made up of a sill which is fed by a vertical pipe and its top is 200m deep. The sediments are overlaying a basement (white area) which is magnetized by induction (with intensity $0.1\,\mathrm{A\,m^{-1}}$) and generates a regional anomaly (not shown). The sedimentary package and basement are semi-infinite along the x axis. The simulated geomagnetic field has inclination $-39.8°$ and declination $-22.5°$. The synthetic intrusion has a reversed magnetization with inclination $I = 39.8°$, declination $D = 157.5°$ and intensity $6\,\mathrm{A\,m^{-1}}$. In this example, the total-field anomaly produced by the intrusion overlaps the one produced by the basement. The total-field anomaly produced by both the intrusion and the basement was calculated on a 100×100 regular grid ($N = 10\,000$), which varies from 0 to 10 km and from 45 to 55 km in x and y directions, respectively, on a plane with constant vertical coordinate -800 m. Figure 11 shows this total-field anomaly contaminated with a pseudo-random Gaussian noise with zero mean and standard deviation equal to 2 nT.

We applied our method to the total-field anomaly shown in Fig. 11 aiming at estimating the magnetization direction of the simulated intrusion (Fig. 10). The position of the synthetic intrusion was estimated by Euler deconvolution. The synthetic intrusion is not an ideal source and does not have a characteristic structural index. In this case, we (wrongly) presumed that the noise-corrupted total-field anomaly is produced by an spherical body and use a structural index equal to 3. Figure 12 shows that the estimated location (black point) obtained by Euler deconvolution is placed outside the synthetic intrusion (red prisms). Even using this poor estimate of the location of the source, our method obtained estimated declinations ($\hat{D}$ and $\tilde{D}$) and inclinations ($\hat{I}$ and $\tilde{I}$) close to the true values (Tab. 4). In practical situations, however, the quality of the estimated magnetization direction may be accessed by using the reduction to the pole. Figure 13 shows that the reduction to the pole calculated with the robust estimate of the magnetization direction (Tab. 4) obtained by our method leads to a predominantly positive anomaly, which is very close to the true one. This result illustrates the robustness of our method when applied to retrieve the magnetization direction of a complex source whose centre is poorly estimated by Euler deconvolution.

4 Application to field data

In Goiás state, central region of Brazil, there are occurrences of Cretaceous alkaline rocks along a lineament NW–SE that have been studied since the 60's. In a broad regional scale study, Almeida (1983) denominated these occurrences as Rio Verde–Iporá Igneous Province. Posteriorly, Sgarbi and Gaspar (2002) grouped the Rio Verde–Iporá Igneous Province and the Alto Paranaíba Igneous Province (between the Goiás and Minas Gerais states, Fig. 14) into the Minas-Goiás Alkaline Province. According to these authors, the Minas-Goiás Alkaline Province would be divided into four sub-provinces: Mata da Corda, Alto do Paranaíba, Iporá and Santo Antônio da Barra. In the same year, Junqueira-Brod et al. (2002) returned to the concept of two distinct provinces. These authors maintained the old name Alto Paranaíba Igneous Province for designating the alkaline rocks located between the Goiás and Minas Gerais states and denominated the alkaline rocks near from Rio Verde and Iporá cities (in the Goiás state) as Goiás Alkaline Province (GAP). Here, we use this nomenclature proposed by Junqueira-Brod et al. (2002).

The GAP is formed by mafic to ultramafic alkaline rocks presenting a wide variety of petrographic types (Almeida, 1983; Junqueira-Brod et al., 2005; Carlson et al., 2007; Marangoni and Mantovani, 2013). Among the main alkaline complexes in the north portion of GAP are the Montes Claros de Goiás, Diorama, Córrego dos Bois, Morro do Macaco and Fazenda Buriti (Fig. 14). These alkaline intrusions are surrounded by Precambrian basement and the Phanerozoic sedimentary rocks of the Paraná basin. In 2004, this region was flown by an aeromagnetic survey at an approximately constant height of $100\,\text{m}$ from the terrain (approximately constant normal height of $500\,\text{m}$). This survey has a flight pattern with N–S lines spaced from $500\,\text{m}$ and E–W tie-lines spaced from $5000\,\text{m}$. Along each line, the data are spaced from approximately $8\,\text{m}$. The data were corrected for diurnal variation and subtracted from the geomagnetic field modelled by using the International Geomagnetic Reference Field (IGRF) evaluated at the 2004.62 epoch, with declination $-18.5°$ and inclination $-19.5°$. This region is characterized by intense total-field anomalies (with notable remnant magnetization) that are generally associated to the alkaline rocks of GAP (Dutra and Marangoni, 2009; Dutra et al., 2012; Marangoni and Mantovani, 2013).

We applied our method to interpret the data located in the area delimited by the red rectangle shown in Fig. 14, near from the alkaline complex of Diorama. The data are shown in Fig. 15. To attenuate the non-dipolar effects present in the data, we applied the Polynomial Equivalent Layer (Oliveira Jr. et al., 2013) to continue the anomaly upward to a constant normal height of $1000\,\text{m}$ in a regularly spaced grid. By inverting the upward continued data (not shown), we estimated the centre of the body by applying the Euler deconvolution and obtained its magnetization direction by using least-squares and robust estimates. We obtained the estimated inclinations $\hat{I} = -69.25595° \pm 0.00013°$ and $\tilde{I} = -71.41751° \pm 0.00182°$ and declinations $\hat{D} = -16.22821° \pm 0.00050°$ and $\tilde{D} = -23.39541° \pm 0.01049°$. The caret ($^\wedge$) and tilde ($^\sim$) denote the results computed by using, respectively, the least-squares and robust estimates.

For verifying the plausibility of the estimated inclinations and declinations, we used them to reduce the observed total-field anomaly (Fig. 15) to the pole. Figure 16 shows that the estimated magnetization directions obtained with the least-squares and robust estimates lead to very confident RTP anomalies, since the dipolar characteristic of observed total-field anomaly (Fig. 15) is almost completely suppressed. ~~We also used this~~

~~By using the~~ estimated magnetization directions ~~for reducing another~~ obtained from the simple dipolar total-field anomaly shown in Fig. 15, we reduced to the pole another complex non-dipolar total-field anomaly (Fig. ~~17)to the pole~~17). This total-field anomaly is located over the Montes Claros de Goiás alkaline complex (Fig. 14), which is near from the alkaline complex of Diorama. Figure 18 shows that this estimated magnetization directions are very good because they yield predominantly positive RTP anomalies. These results show that the magnetization direction of the sources in the alkaline complex of Montes Claros de Goiás are very close to that ones estimated from the total-field anomaly (Fig. 15) near from the alkaline complex of Diorama, suggesting that these sources emplaced at depth within almost the same geological time interval. Notice that in this

field-data application, the result obtained from inverting a small piece of the data set shed a light on this complex geological setting.

5   Conclusions

We present a computationally effective method for estimating the magnetization direction of multiple sources with approximately spherical shapes by inverting the total-field anomaly produced by them. Our method assumes that the sources have uniform magnetization and that the positions of their centres are known. Prior knowledge about the source sizes is not required. Our method can be applied for ~~interpreting~~ determining the average magnetization direction within multiple sources with different magnetization directions. Besides, it can be directly applied to interpret irregularly spaced total-field anomaly data measured on uneven surfaces and requires no prior transformation like reduction to the pole, total gradient or total magnitude anomalies. The method also contains flexibility to be implemented in two different numerical approaches. The first one is based on the minimization of the L2-norm of the residuals between the observed and predicted total-field anomalies. This approach results in a linear inverse problem for obtaining a least-squares estimate of the magnetization vector components of the sources. The second approach is based on the minimization of the L1-norm of the residuals between the observed and predicted total-field anomalies, leading to a non-linear inverse problem for obtaining a robust estimate of the magnetization vector components of the sources.

The results obtained with the synthetic data simulating a spherical source with known centre show the good performance of our method in retrieving the true magnetization direction. Tests with synthetic data produced by simulated sources that violates the premisses assumed by our method show the robustness of our method against interfering anomalies and against errors in the location of the centre of the source. The results show that our method is sensitive to errors in the horizontal location of the centre of the source. On the other hand, it is insensitive to errors in the depth of the centre of the source. Additionally, we show how the upward continuation can be used to make possible the application of our method for interpreting non-spherical sources producing total-field anomalies with non-dipolar features. These non-dipolar features can greatly affect the results obtained with the least-squares estimate, especially when the data are near from the source. Applications to field data over the Goiás Alkaline Province (GAP), Brazil, show that our method can be a powerful tool for interpreting real geological scenarios. Our estimates near from the alkaline complex of Diorama, suggest the presence of non-outcropping sources with strong remanent magnetization, corroborating previous works. This estimated magnetization direction leads to very plausible RTP anomalies not only over the region

near from the complex of Diorama, but also over the alkaline complex of Montes Claros de Goiás. These results show that the non-outcropping sources near from the alkaline complex of Diorama have almost the same magnetization direction of that ones in the alkaline complex of Montes Claros de Goiás, strongly suggesting that these sources have emplaced at depth within almost the same geological time interval.

Although the upward continuation seems to be useful for overcoming the difficulties in the interpretation of strongly non-dipolar total-field anomalies, there will always be a limit for using this technique. The interpreter should always verify the quality of the estimated magnetization direction by using, for example, a reduction to the pole. One might think that the high sensitivity of our method to uncertainties in the horizontal coordinates of the centres of the sources is a drawback. This is not true because these coordinates are generally well estimated by the Euler deconvolution. The high sensitivity of our method to errors in horizontal location of the centre of the sources suggests that the horizontal coordinates of the sources' centres could also be estimated by inversion. On the other hand, the insensitivity our method to errors in the depth of the sources suggests that the sources' depth could not be easily estimated by inversion and would need some a priori information.

References

Almeida, F. F. M.: Relações tectônicas das rochas alcalinas mesozóicas da região meridional da plataforma sul-americana, Revista Brasileira de Geociências, 13, 139–158, 1983.

Aster, R. C., Borchers, B., and Thurber, C. H.: Parameter Estimation and Inverse Problems (International Geophysics), Academic Press, 2005.

Baranov, V.: A new method for interpretation of aeromagnetic maps: Pseudo-gravimetric anomalies, Geophysics, 22, 359–382, doi:10.1190/1.1438369, 1957.

Baranov, V. and Naudy, H.: Numerical calculation of the formula of reduction to the magnetic pole, Geophysics, 29, 67–79, doi:10.1190/1.1439334, 1964.

Barbosa, V. C. F. and Silva, J. B. C.: Interactive 2D magnetic inversion: A tool for aiding forward modeling and testing geologic hypotheses, Geophysics, 71, L43–L50, doi:10.1190/1.2258093, 2006.

Bard, Y.: Nonlinear Parameter Estimation, Academic Press, 1973.

Bhattacharyya, B. K.: A method for computing the total magnetization vector and the dimensions of a rectangular block-shaped body from magnetic anomalies, Geophysics, 31, 74–96, doi:10.1190/1.1439765, 1966.

Blakely, R. J.: Potential Theory in Gravity and Magnetic Applications, Cambridge University Press, 1996.

Carlson, R. W., Araujo, A. L. N., Junqueira-Brod, T. C., Gaspar, J. C., Brod, J. A., Petrinovic, I. A., Hollanda, M. H. B., Pimentel, M. M., and Sichel, S.: Chemical and isotopic relationships between peridotite xenoliths and mafic–ultrapotassic rocks from Southern Brazil, Chemical Geology, 242, 415 – 434, doi:10.1016/j.chemgeo.2007.04.009, 2007.

Clark, D. A.: Methods for determining remanent and total magnetisationsof magnetic sources – a review, Explor. Geopphys., pp. 271–304, doi:10.1071/EG14013, 2014.

Dannemiller, N. and Li, Y.: A new method for determination of magnetization direction, Geophysics, 71, L69–L73, doi:10.1190/1.2356116, 2006.

Dutra, A. C. and Marangoni, Y. R.: Gravity and magnetic 3D inversion of Morro do Engenho complex, Central Brazil, Journal of South American Earth Sciences, 28, 193 – 203, doi:10.1016/j.jsames.2009.02.006, 2009.

Dutra, A. C., Marangoni, Y. R., and Junqueira-Brod, T. C.: Investigation of the Goiás Alkaline Province, Central Brazil: Application of gravity and magnetic methods, Journal of South American Earth Sciences, 33, 43 – 55, doi:10.1016/j.jsames.2011.06.004, 2012.

Ellis, R. G., de Wet, B., and Macleod, I. N.: Inversion of magnetic data for remanent and induced sources, ASEG Extended Abstracts, pp. 1–4, doi:10.1071/ASEG2012ab117, 2012.

Emilia, D. and Massey, R.: Magnetization estimation for nonuniformly magnetized seamounts, Geophysics, 39, 223–231, doi:10.1190/1.1440423, 1974.

Farquharson, C. G. and Oldenburg, D. W.: Non-linear inversion using general measures of data misfit and model structure, Geophys. J. Int., 134, 213–227, doi:10.1046/j.1365-246x.1998.00555.x, 1998.

Fedi, M., Florio, G., and Rapolla, A.: A method to estimate the total magnetization direction from a distortion analysis of magnetic anomalies1, Geophys. Prospect., 42, 261–274, doi:10.1111/j.1365-2478.1994.tb00209.x, 1994.

Fornasini, P.: The Uncertainty in Physical Measurements: An Introduction to Data Analysis in the Physics Laboratory, Springer, 2008.

Gerovska, D., Araúzo-Bravo, M. J., and Stavrev, P.: Estimating the magnetization direction of sources from southeast Bulgaria through correlation between reduced-to-the-pole and total magnitude anomalies, Geophys. Prospect., 57, 491–505, doi:10.1111/j.1365-2478.2008.00761.x, 2009.

Helbig, K.: Some integrals of magnetic anomalies and their relation to the parameters of the disturbing body, Zeitschrift für Geophysik, 29, 83–96, 1963.

Hunter, J. D.: Matplotlib: A 2D graphics environment, Computing in Science & Engineering, 9, 90–95, doi:10.1109/MCSE.2007.55, http://doi.ieeecomputersociety.org/10.1109/mcse.2007.55, 2007.

Junqueira-Brod, T. C., Roig, H. L., Gaspar, J. C., Brod, J. A., and Meneses, P. R.: A Província Alcalina de Goiás e a extensão do seu vulcanismo kamafugítico, Revista Brasileira de Geociências, 32, 559–566, 2002.

Junqueira-Brod, T. C., Gaspar, J. C., Brod, J. A., and Kafino, C. V.: Kamafugitic diatremes: their textures and field relationships with examples from the Goiás alkaline province, Brazil, Journal of South American Earth Sciences, 18, 337–353, doi:10.1016/j.jsames.2004.11.002, 2005.

Kubota, R. and Uchiyama, A.: Three-dimensional magnetization vector inversion of a seamount, Earth Planets Space, 57, 691–699, doi:10.1186/BF03351849, 2005.

Langel, R. A. and Hinze, W. J.: The Magnetic Field of the Earth's Lithosphere: The Satellite Perspective, Cambridge University Press, 1998.

Lelièvre, P. G. and Oldenburg, D. W.: A 3D total magnetization inversion applicable when significant, complicated remanence is present, Geophysics, 74, L21–L30, doi:10.1190/1.3103249, 2009.

Li, X.: Understanding 3D analytic signal amplitude, Geophysics, 71, L13–L16, doi:10.1190/1.2184367, 2006.

Li, Y. and Oldenburg, D. W.: 3-D inversion of magnetic data, Geophysics, 61, 394–408, doi:10.1190/1.1443968, 1996.

Marangoni, Y. R. and Mantovani, M. S.: Geophysical signatures of the alkaline intrusions bordering the Paraná Basin, Journal of South American Earth Sciences, 41, 83–98, doi:10.1016/j.jsames.2012.08.004, 2013.

Medeiros, W. E. and Silva, J. B. C.: Simultaneous estimation of total magnetization direction and 3-D spatial orientation, Geophysics, 60, 1365–1377, doi:10.1190/1.1443872, 1995.

Melo, F., Barbosa, V., Uieda, L., Oliveira Jr., V., and Silva, J.: Estimating the nature and the horizontal and vertical positions of 3D magnetic sources using Euler deconvolution, Geophysics, 78, J87–J98, doi:10.1190/geo2012-0515.1, 2013.

Menke, W.: Geophysical Data Analysis: Discrete Inverse Theory (International Geophysics), Academic Press, 1989.

Nabighian, M.: The analytic signal of two-dimensional magnetic bodies with polygonal cross- section: its properties and use for automated anomaly interpretation, Geophysics, 37, 507–517, doi:10.1190/1.1440276, 1972.

Nabighian, M.: Additional comments on the analytic signal of two-dimensional magnetic bodies with polygonal cross-section, Geophysics, 39, 85–92, doi:10.1190/1.1440416, 1974.

Nabighian, M.: Toward a three-dimensional automatic interpretation of potential field data via generalized Hilbert transforms: Fundamental relations, Geophysics, 49, 780–786, doi:10.1190/1.1441706, 1984.

Nabighian, M., Grauch, V., Hansen, R., LaFehr, T., Li, Y., Peirce, J., Phillips, J., and Ruder, M.: The historical development of the magnetic method in exploration, Geophysics, 70, 33ND–61ND, doi:10.1190/1.2133784, 2005.

Oliveira Jr., V. C., Barbosa, V. C. F., and Uieda, L.: Polynomial equivalent layer, Geophysics, 78, G1–G13, doi:10.1190/geo2012-0196.1, 2013.

Parker, R. L., Shure, L., and Hildebrand, J. A.: The application of inverse theory to seamount magnetism, Rev. Geophys., 25, 17–40, doi:10.1029/RG025i001p00017, 1987.

Pérez, F. and Granger, B. E.: IPython: a System for Interactive Scientific Computing, Computing in Science and Engineering, 9, 21–29, doi:10.1109/MCSE.2007.53, http://ipython.org, 2007.

Phillips, J. D.: Can we estimate total magnetization directions from aeromagnetic data using Helbig's integrals?, Earth, Planets and Space, 57, 681–689, 2005.

Pilkington, M.: 3-D magnetic imaging using conjugate gradients, Geophysics, 62, 1132–1142, doi:10.1190/1.1444214, 1997.

Portniaguine, O. and Zhdanov, M. S.: Focusing geophysical inversion images, Geophysics, 64, 874–887, doi:10.1190/1.1444596, 1999.

Portniaguine, O. and Zhdanov, M. S.: 3-D magnetic inversion with data compression and image focusing, Geophysics, 67, 1532–1541, doi:10.1190/1.1512749, 2002.

Ramachandran, P. and Varoquaux, G.: Mayavi: 3D visualization of scientific data, Computing in Science & Engineering, 13, 40–51, doi:10.1109/MCSE.2011.35, http://ieeexplore.ieee.org/xpls/abs_all.jsp?arnumber=5725237, 2011.

Reid, A., Allsop, J., Granser, H., Millett, A., and Somerton, I.: Magnetic interpretation in three dimensions using Euler deconvolution, Geophysics, 55, 80–91, doi:10.1190/1.1442774, 1990.

Reid, A. B., Ebbing, J., and Webb, S. J.: Avoidable Euler Errors – the use and abuse of Euler deconvolution applied to potential fields, Geophysical Prospecting, doi:10.1111/1365-2478.12119, 2014.

Roest, W. R. and Pilkington, M.: Identifying remanent magnetization effects in magnetic data, Geophysics, 58, 653–659, doi:10.1190/1.1443449, 1993.

Scales, J. A., Gerztenkorn, A., and Treitel, S.: Fast Lp Solution of Large, Sparse, Linear Systems: Application to Seismic Travel Time Tomography, J. Comp. Phys., 75, 314–333, doi:10.1016/0021-9991(88)90115-5, 1988.

Sgarbi, P. B. A. and Gaspar, J. C.: Geochemistry of Santo Antônio da Barra Kamafugites, Goiás, Brazil, Journal of South American Earth Sciences, 14, 889–901, doi:10.1016/S0895-9811(01)00079-7, 2002.

Silva, J. and Barbosa, V.: 3D Euler deconvolution: Theoretical basis for automatically selecting good solutions, Geophysics, 68, 1962–1968, doi:10.1190/1.1635050, 2003.

Silva, J. B. C.: Reduction to the pole as an inverse problem and its application to low-latitude anomalies, Geophysics, 51, 369–382, doi:10.1190/1.1442096, 1986.

Telford, W. M., Geldart, L. P., and Sheriff, R. E.: Applied Geophysics, Cambridge University Press, 1990.

Thompson, D.: EULDPH: A new technique for making computer-assisted depth estimates from magnetic data, Geophysics, 47, 31–37, doi:10.1190/1.1441278, 1982.

Tontini, F. C. and Pedersen, L. B.: Interpreting magnetic data by integral moments, Geophys. J. Int., 174, 815–824, doi:10.1111/j.1365-246X.2008.03872.x, 2008.

Twomey, S.: Introduction to the Mathematics of Inversion in Remote Sensing and Indirect Measurements, Dover Publications, Inc., 1977.

Uieda, L., Oliveira Jr., V. C., and Barbosa, V. C. F.: Geophysical tutorial: Euler deconvolution of potential-field data, The Leading Edge, 33, 448–450, doi:10.1190/tle33040448.1, 2014.

Table 1. Test with the synthetic data (Fig. 3a) produced by a sphere and a rectangular prism. Comparison between the estimated and true values of the magnetization declination D and inclination I. The uncertainties σ_D and σ_I (shown between parenthesis) are calculated by using Eqs. (34) and (35). All values are in degree (°). We use a caret ($\wedge$) and a tilde ($\sim$) to distinguish the quantities computed by using, respectively, the least-squares $\hat{\boldsymbol{h}}$ and robust $\tilde{\boldsymbol{h}}$ estimates.

	Sphere		Prism	
D	−10.00000	~	−40.00000	~
$\hat{D}$	−10.07141	(0.00001)	−40.63733 $\hat{\sigma}_\mathrm{D}$	0.00000 (0.00113)
$\tilde{D}$	−10.03229	−40.24585 $\tilde{\sigma}_\mathrm{D}$ (0.00130)	−40.24585	(0.03601)
I	−20.00000	~	30.00000	~
$\hat{I}$	−19.99437	(0.00001)	31.04075 $\hat{\sigma}_\mathrm{I}$	0.00000 (0.00068)
$\tilde{I}$	−20.01263	30.60551 $\tilde{\sigma}_\mathrm{I}$ (0.00042)	30.60551	(0.02047)

Table 2. Test with the synthetic data (Fig. 3b) produced by a sphere and a rectangular prism. Comparison between the estimated and true values of the magnetization declination D and inclination I. The uncertainties σ_D and σ_I (shown between parenthesis) are calculated by using Eqs. (34) and (35). All values are in degree (°). We use a caret ($\wedge$) and a tilde ($\sim$) to distinguish the quantities computed by using, respectively, the least-squares $\hat{\boldsymbol{h}}$ and robust $\tilde{\boldsymbol{h}}$ estimates.

	Sphere		Prism	
D	−10.00000	~	−40.00000	~
$\hat{D}$	−4.28547	(0.00001)	−23.63607 $\hat{\sigma}_\mathrm{D}$	0.00000 (0.00130)
$\tilde{D}$	−8.73648	−39.37397 $\hat{\sigma}_\mathrm{D}$ (0.00135)	−39.37397	(0.03679)
I	−20.00000	~	30.00000	~
$\hat{I}$	−25.11757	(0.00001)	39.08012 $\hat{\sigma}_\mathrm{I}$	0.00000 (0.00064)
$\tilde{I}$	−21.75674	33.40926 $\tilde{\sigma}_\mathrm{I}$ (0.00027)	33.40926	(0.01648)

Table 3. Test with synthetic data (Fig. 9) showing strong-interfering anomalies. Comparison between the estimated and true values of the magnetization declination D and inclination I. The uncertainties σ_D and σ_I (shown between parenthesis) are calculated by using Eqs. (34) and (35). All values are in degree (°). We use a caret ($\wedge$) and a tilde ($\sim$) to distinguish the quantities computed by using, respectively, the least-squares $\hat{\boldsymbol{h}}$ and robust $\tilde{\boldsymbol{h}}$ estimates.

	Eastern prism		Western prism	
D	−23.41322	~	23.41322	~
$\hat{D}$	−31.45370	(0.00008)	30.67233	(0.00875)
$\tilde{D}$	−26.57707	(0.01778)	25.25037	(0.13333)
I	−7.54509	~	−7.54509	~
$\hat{I}$	−9.23914	(0.00004)	−9.06131	(0.00628)
$\tilde{I}$	−7.98897	(0.00408)	−11.05456	(0.06386)

Table 4. Test with synthetic data (Fig. 11) produced by a complex geological scenario. Comparison between the estimated and true values of the magnetization declination D and inclination I. The uncertainties σ_D and σ_I (shown between parenthesis) are calculated by using Eqs. (34) and (35). All values are in degree (°). We use a caret ($\wedge$) and a tilde ($\sim$) to distinguish the quantities computed by using, respectively, the least-squares $\hat{\boldsymbol{h}}$ and robust $\tilde{\boldsymbol{h}}$ estimates.

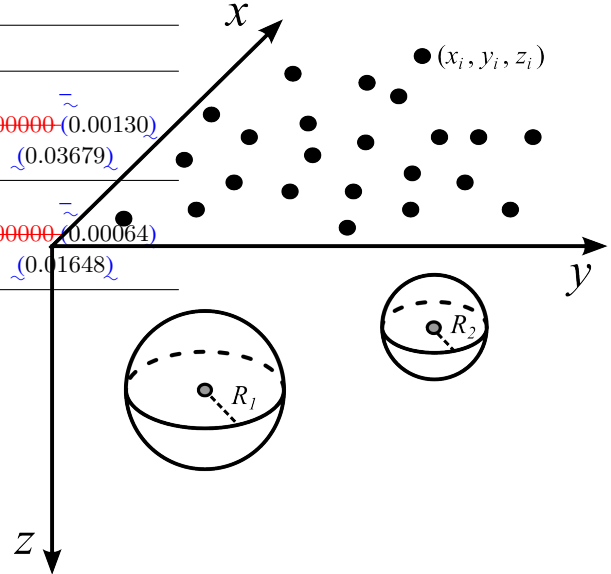|	Synthetic intrusion	
D	157.50000	~
$\hat{D}$	167.39501	(0.00060)
$\tilde{D}$	164.19461	(0.02669)
I	39.80000	~
$\hat{I}$	37.33816	(0.00035)
$\tilde{I}$	39.99470	(0.00939)

Fig. 1. Schematic representation of $L = 2$ spheres uniformly magnetized at the subsurface. These spheres have radii R_j (dashed straight lines), constant magnetization vectors $\boldsymbol{m}^j$ and centres (grey dots) at (xc_j, yc_j, zc_j), $j = 1, \ldots, L$. The magnetic effect produced by these spheres can be observed at the points (x_i, y_i, z_i), $i = 1, \ldots, N$ (black dots). In this Cartesian coordinate system, x points to the geographic North, y points to East and z points downward.
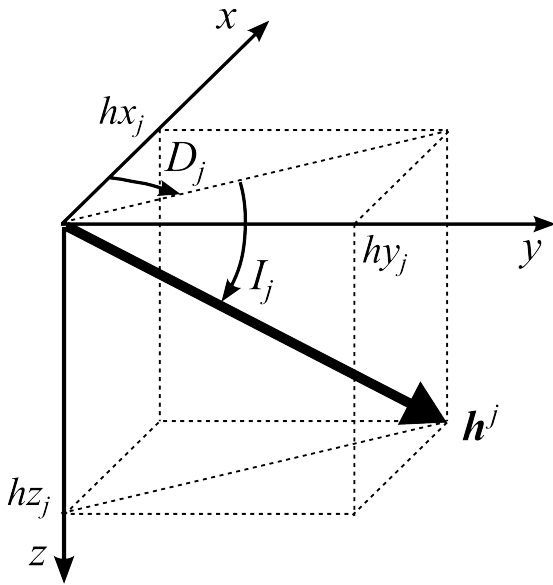
Fig. 2. Schematic representation of the vector $\boldsymbol{h}^j$ (Eq. 12) with elements hx_j, hy_j and hz_j in Cartesian coordinates. This vector has a declination D_j (positive in the clockwise sense) and inclination I_j (positive downward), $j = 1, \ldots, L$.
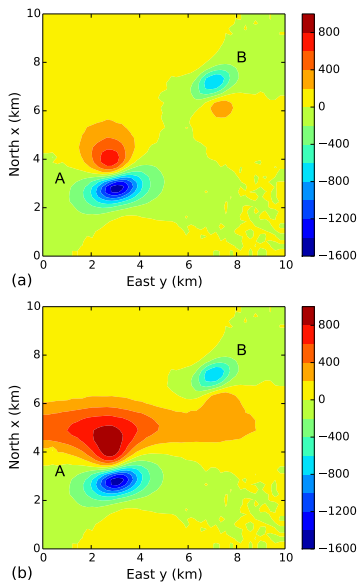

Fig. 3. Validation test and robustness against interfering anomalies. **(a)** Synthetic noise-corrupted total field anomaly produced (nT) by a sphere and a rectangular prism. **(b)** Synthetic anomaly shown in **(a)** plus produced by an interfering anomaly. The anomalies produced by the sphere and prism are pinpointed as (A) and (B), respectively.
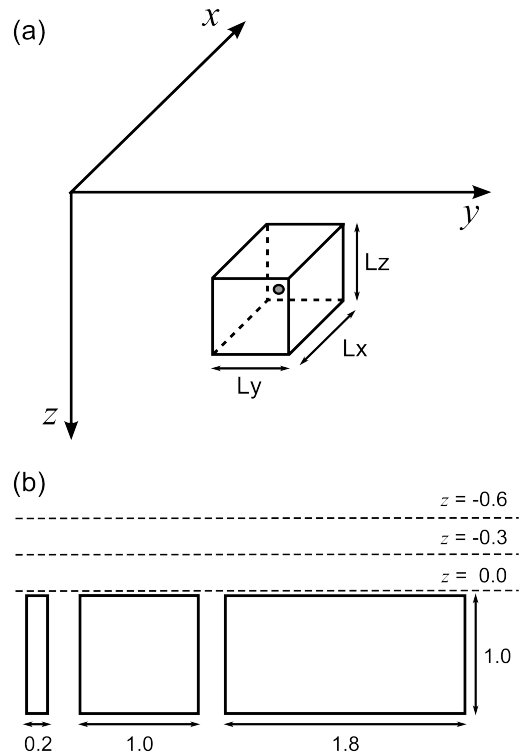
Fig. 4. Robustness against non-spherical sources. **(a)** Rectangular prism with dimensions Lx, Ly and Lz and centre at the grey dot. **(b)** Projection of three prisms on the plane yz. All prisms have top at $z = 10\,\mathrm{m}$ and side lengths $Lx = Lz = 1000\,\mathrm{m}$. The horizontal dimension Ly of each prism is equal to $200\,\mathrm{m}$, $1000\,\mathrm{m}$ and $1800\,\mathrm{m}$. The dashed lines represent the vertical coordinate z of three different horizontal planes above the prisms. For convenience, all coordinates and lengths are normalized by the numerical value of Lz ($1000\,\mathrm{m}$) to obtain dimensionless quantities.
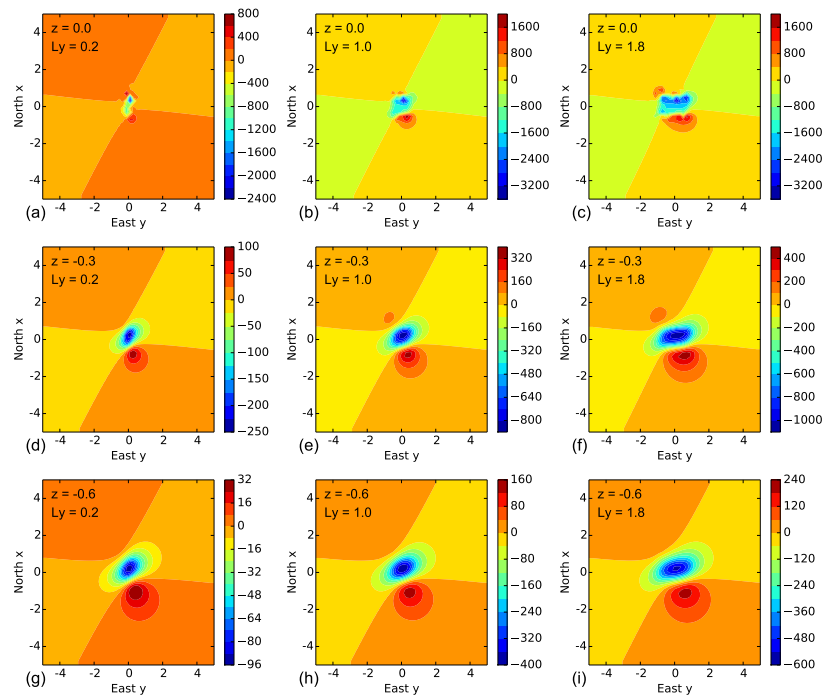
Fig. 5. Robustness against non-spherical sources. Noise-corrupted total-field anomaly produced by each one of the three rectangular prisms shown in Fig. 4b on three horizontal planes with different constant vertical coordinates z (dashed lines in Fig. 4b). We consider that the centre of all prisms are located at $xc = 0.00$, $yc = 0.00$ and $zc = 0.51$. The intensity, declination and inclination of the magnetization vector of all prisms are equal to $6\,\mathrm{A\,m^{-1}}$, $-40°$ and $30°$, respectively. The simulated geomagnetic field is constant, with declination $-15°$ and inclination $-10°$. The data are in nT and all coordinates and lengths are dimensionless (see Fig. 4).
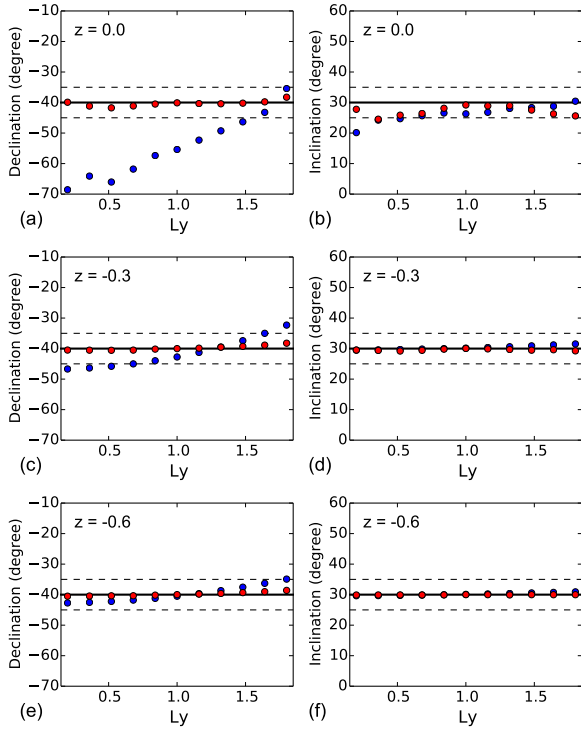
Fig. 6. Robustness against non-spherical sources. The blue and red dots represent, respectively, the results obtained with the least-squares $\hat{\boldsymbol{h}}$ (Eq. 19) and robust $\tilde{\boldsymbol{h}}$ (Eqs. 21 and 22) estimates. Each dot represents an estimated declination or inclination obtained from the total-field anomaly produced by a rectangular prism with a different Ly (Fig. 4). z indicates the constant vertical coordinate of the planar surface on which the total-field anomaly was calculated (dashed lines in Fig. 4b). The continuous black lines represent the true declinations (or inclinations). The dashed lines represent the true declination (or inclination) $\pm 5°$.
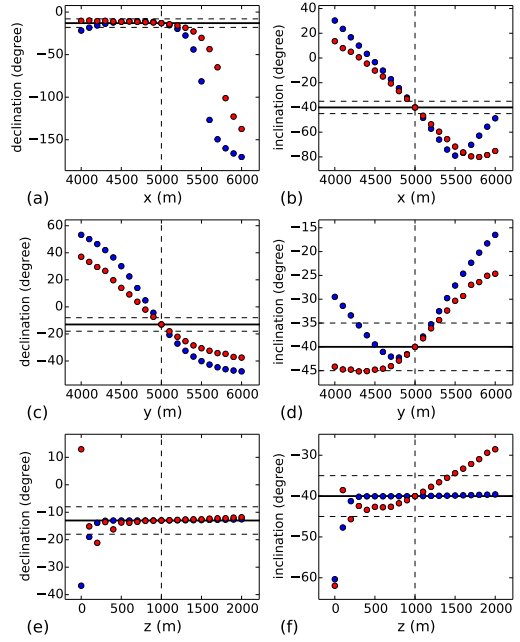
Fig. 7. Robustness against errors in the centre location. The blue and red dots represent, respectively, the magnetization direction of a simulated spherical body obtained with the least-squares $\hat{\boldsymbol{h}}$ (Eq. 19) and robust $\tilde{\boldsymbol{h}}$ (Eqs. 21 and 22) estimates. The estimated declinations and inclinations were obtained by presuming different positions for the centre of the source along the x, y and z axis. Along each axis, the magnetization direction was estimated by considering 21 different centres regularly spaced in a range of $2000\,\mathrm{m}$ on a line passing through the right coordinates of the centre of the simulated spherical body (vertical dashed lines). The continuous black lines represent the true declinations (or inclinations). The dashed lines represent the true declination (or inclination) $\pm 5°$.
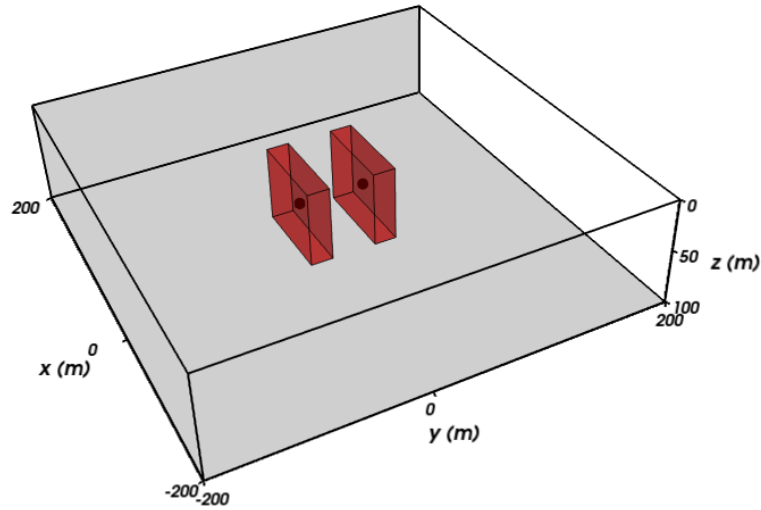
Fig. 8. ~~Application to field data on the Gois Alkaline Province~~ Strong-interfering anomalies. Synthetic prisms (~~GAP~~ in red) with side lengths equal to 80 m, ~~Brazil. Simplified geological map of~~ 20 m and 70 m along the ~~study area~~ x, which is represented by y and z directions, respectively. Both prisms have a ~~red dot in the inset map~~ depth of ~~Brazil~~ the top at $z = 10$ m. The ~~inset also shows~~ eastern prism has its centre at $xc = 0$ m, $yc = -30$ m and $zc = 45$ m while western prism has its centre shifted 60 m in the ~~Gois~~ positive y direction (~~dark grey area~~ pinpointed black dots) ~~and Minas Gerais (light grey area) states. The total-field anomaly over the area delimited by the red rectangle is shown in Fig. 15. The coordinates are referred to the WGS84 datum. The numbers indicate the main alkaline complexes in this region: 1 – Montes Claros de Gois, 2 – Diorama, 3 – Crrego dos Bois, 4 – Morro do Macaco and 5 – Fazenda Buriti.~~
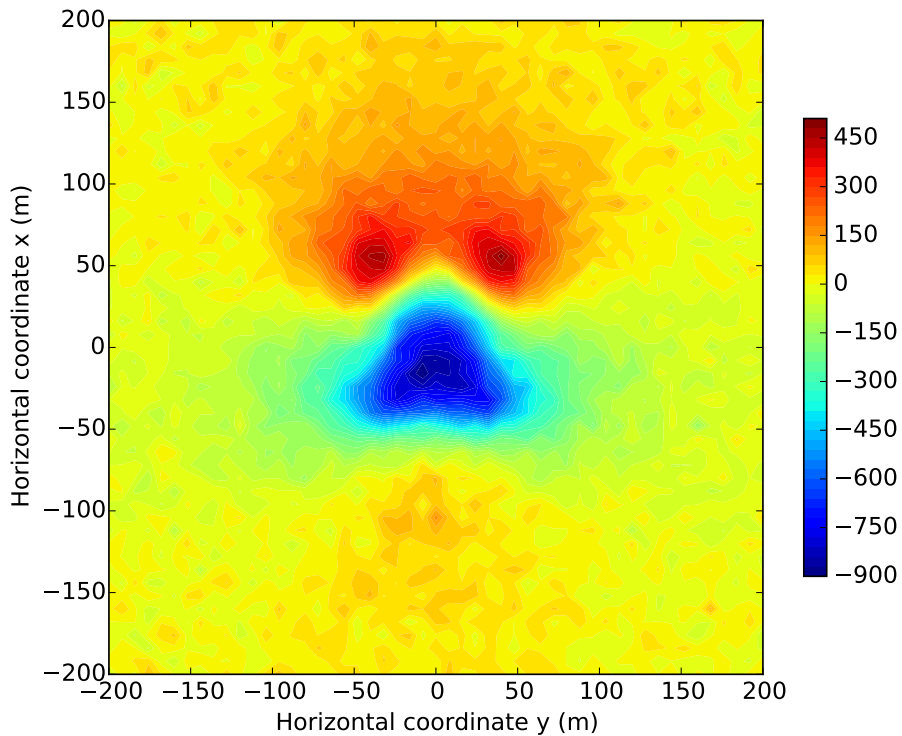
Fig. 9. Strong-interfering anomalies. Noise-corrupted total-field anomaly produced by the synthetic bodies shown in Fig. 8. The data are in nT and were calculated on a plane with constant vertical coordinate equal to -10 m.
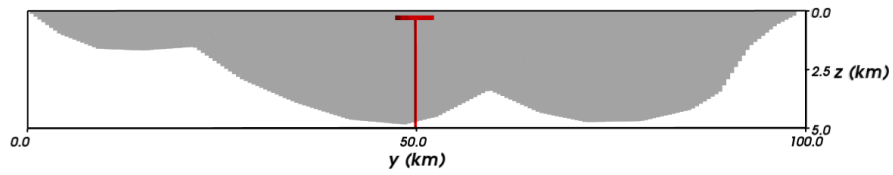
Fig. 10. Igneous intrusion. 2D schematic representation of a synthetic geologic setting composed of a nonmagnetic sedimentary package (in grey), an igneous intrusion (in red) and a basement (in white). The sedimentary package and basement are semi-infinite along the x axis. The basement is magnetized by induction and the intrusion has a strong reversed magnetization. The plot has vertical exaggeration.
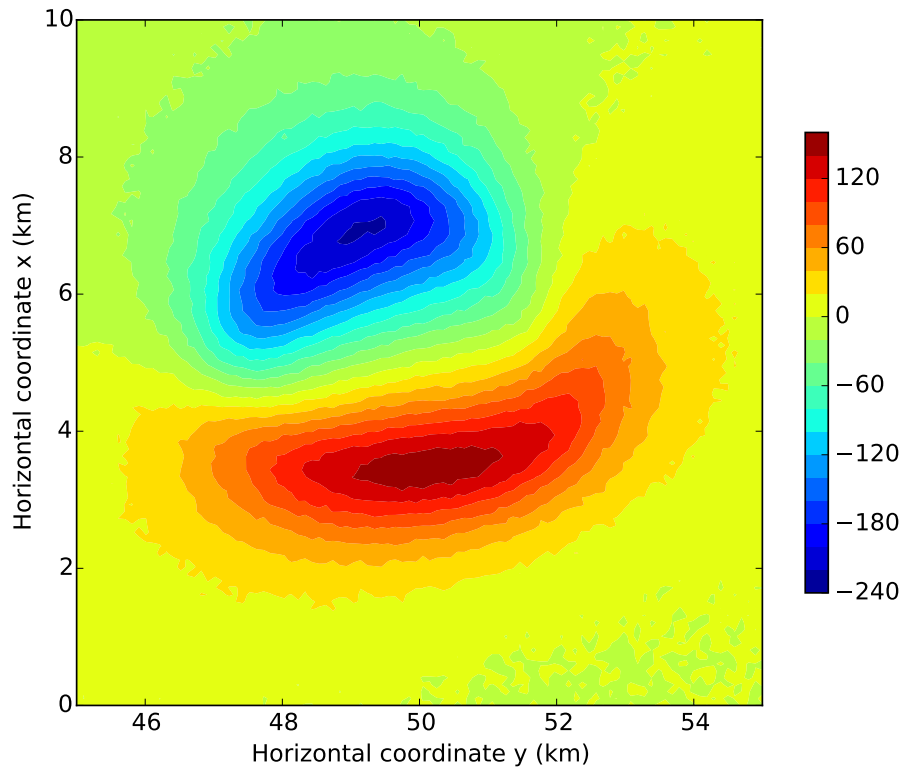

Fig. 11. Igneous intrusion. Noise-corrupted total-field anomaly produced by the synthetic bodies shown schematically in Fig. 10. The data are in nT.
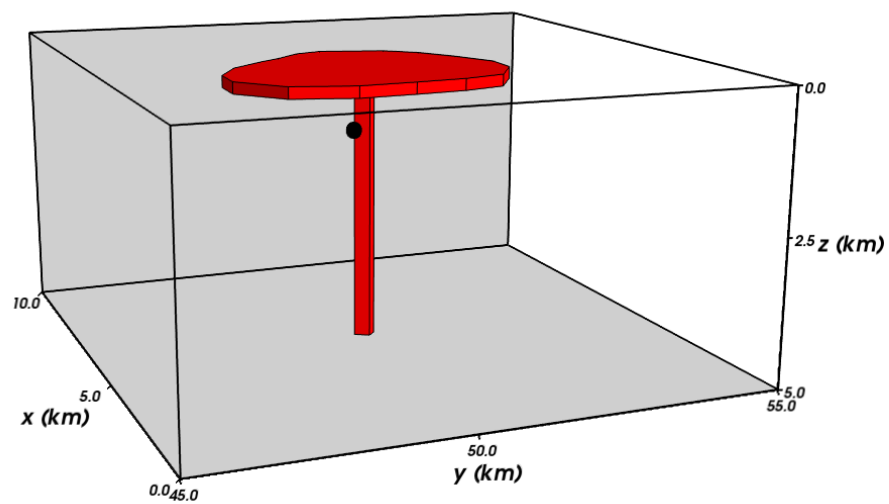
Fig. 12. Igneous intrusion. 3D view of the intrusion (red prisms) and the estimate of the intrusion position by using Euler deconvolution (black point) with a structural index equal to 3. Notice that the Euler solution falls outside the intrusion.
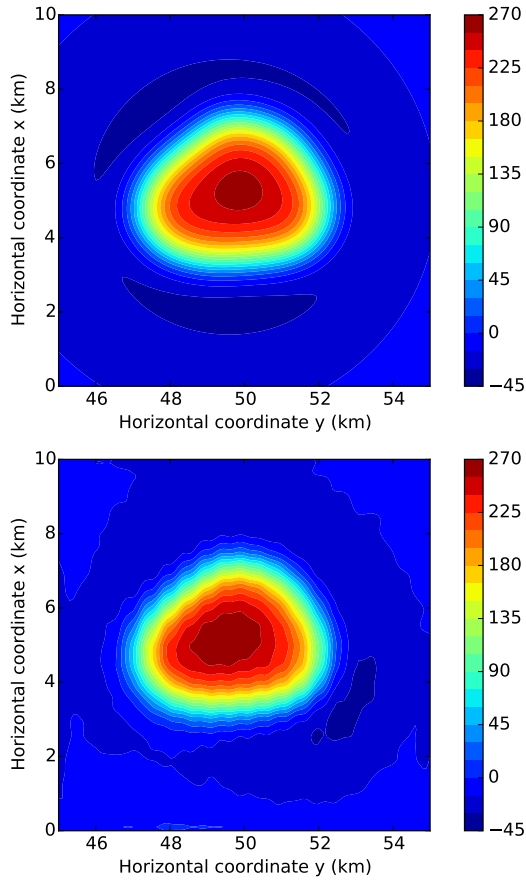
Fig. 13. Igneous intrusion. The upper panel shows the true reduced-to-the-pole anomaly produced by the synthetic bodies shown in Fig. 10. The lower panel shows the reduced-to-the-pole anomaly obtained from the noise-corrupted total-field anomaly shown in Fig. 11. These anomalies were calculated at the same points of the total-field anomaly shown in Fig. 11. The reduction to the pole was calculated by using the robust estimates of declination $\tilde{D}$ and inclination $\tilde{I}$ shown in Tab. 4.
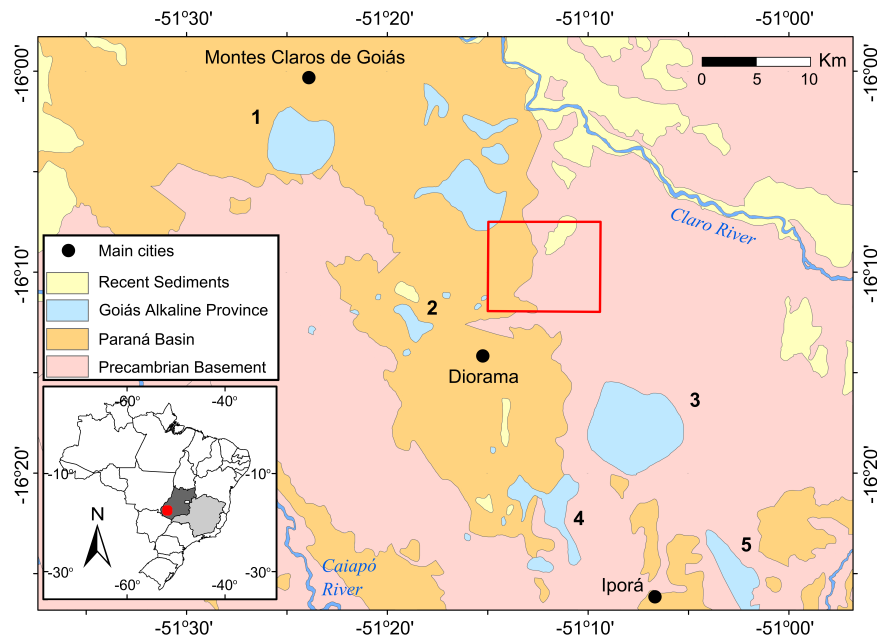
Fig. 14. Application to field data on the Goiás Alkaline Province (GAP), Brazil. Simplified geological map of the study area, which is shown as a red dot in the inset map of Brazil. The inset also shows the Goiás (dark grey area) and Minas Gerais (light grey area) states. The total-field anomaly over the area delimited by the red rectangle is shown in Fig. 15. The coordinates are referred to the WGS84 datum. The numbers indicate the main alkaline complexes in this region: 1 – Montes Claros de Goiás, 2 – Diorama, 3 – Córrego dos Bois, 4 – Morro do Macaco and 5 – Fazenda Buriti.
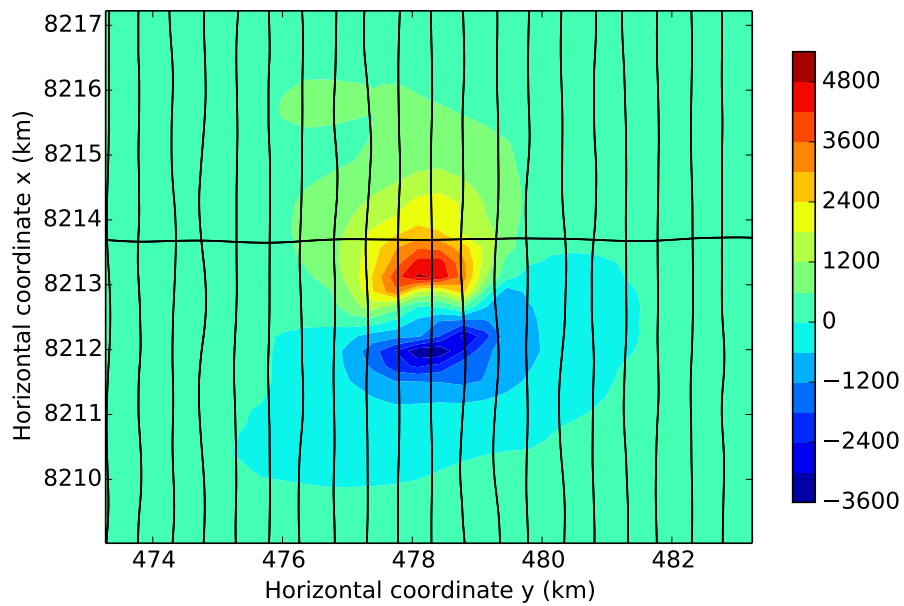
Fig. 15. Application to field data on the Goiás Alkaline Province (GAP), Brazil. Total-field anomaly observed over the area delimited by the red rectangle in Fig. 14. The flight lines of the aeromagnetic survey are shown in black. The magnetic data are in nT and the coordinates are in UTM on the SAD-69 datum, with central meridian $51°$ W. The origins of the east and north coordinates are 500 and 10 000 km, respectively.
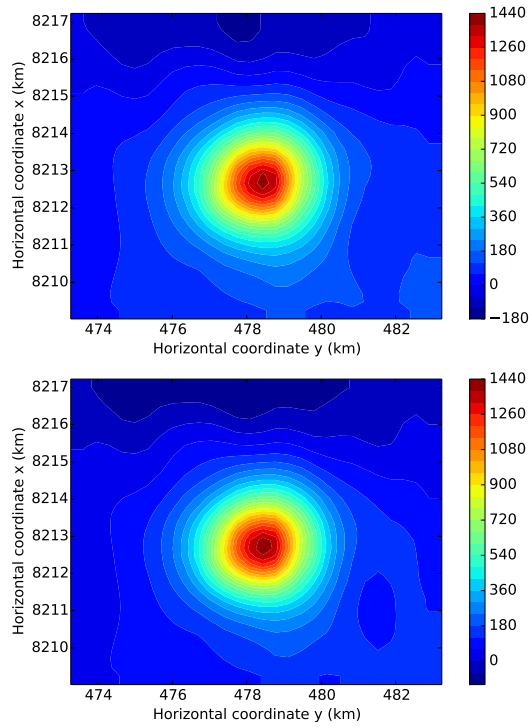
Fig. 16. Application to field data on the Goiás Alkaline Province (GAP), Brazil. Observed total-field anomaly (Fig. 15) reduced to the pole. The upper and lower panels show the RTP anomalies computed by using, respectively, the estimated magnetization direction obtained with the least-squares (inclination $\hat{I} = -69.25595° \pm 0.00013°$ and declination $\hat{D} = -16.22821° \pm 0.00050°$) and robust (inclination $\tilde{I} = -71.41751° \pm 0.00182°$ and declination $\tilde{D} = -23.39541° \pm 0.01049°$) estimates.
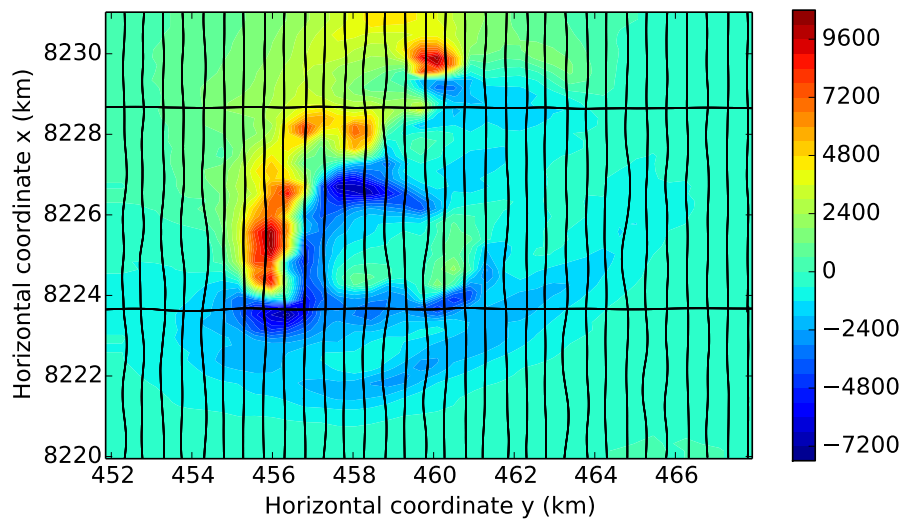
Fig. 17. Application to field data on the Goiás Alkaline Province (GAP), Brazil. Total-field anomaly observed over the Montes Claros de Goiás alkaline complex (Fig. 14). The flight lines of the aeromagnetic survey are shown in black. The magnetic data are in nT and the coordinates are in UTM on the SAD-69 datum, with central meridian $51°$ W. The origins of the east and north coordinates are 500 km and $10\,000$ km, respectively.
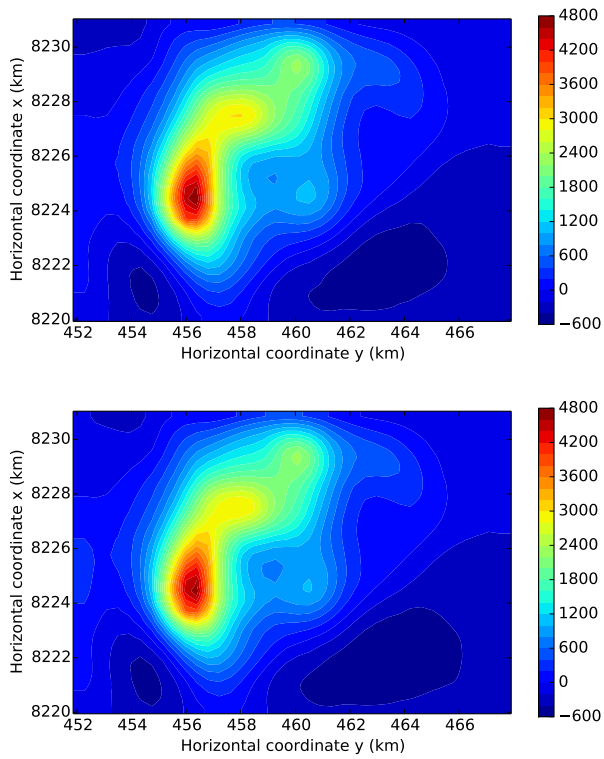
Fig. 18. Application to field data on the Goiás Alkaline Province (GAP), Brazil. Observed total-field anomaly (Fig. 17) reduced to the pole. The upper and lower panels show the RTP anomalies computed by using, respectively, the estimated magnetization direction obtained with the least-squares (inclination $\hat{I} = -69.25595° \pm 0.00013°$ and declination $\hat{D} = -16.22821° \pm 0.00050°$) and robust (inclination $\tilde{I} = -71.41751° \pm 0.00182°$ and declination $\tilde{D} = -23.39541° \pm 0.01049°$) estimates.